

RESEARCH ARTICLE

10.1002/2013JA019388

Special Section:

Fundamental Properties and Processes of Magnetotails

Key Points:

- New plasma data show velocities for 29 kronian plasmoids
- Reconnection at Saturn more commonly observed at dawn than dusk
- Examples of both loop-like and flux rope-like plasmoids presented

Correspondence to:

C. M. Jackman,
c.jackman@soton.ac.uk

Citation:

Jackman, C. M., et al. (2014), Saturn's dynamic magnetotail: A comprehensive magnetic field and plasma survey of plasmoids and traveling compression regions and their role in global magnetospheric dynamics, *J. Geophys. Res. Space Physics*, 119, 5465–5494, doi:10.1002/2013JA019388.

Received 30 AUG 2013

Accepted 3 JUN 2014

Accepted article online 9 JUN 2014

Published online 9 JUL 2014

Saturn's dynamic magnetotail: A comprehensive magnetic field and plasma survey of plasmoids and traveling compression regions and their role in global magnetospheric dynamics

C. M. Jackman^{1,2,3}, J. A. Slavin⁴, M. G. Kivelson^{4,5}, D. J. Southwood⁶, N. Achilleos^{1,2}, M. F. Thomsen⁷, G. A. DiBraccio⁴, J. P. Eastwood⁶, M. P. Freeman⁸, M. K. Dougherty⁶, and M. F. Vogt^{9,10}

¹Department of Physics and Astronomy, University College London, London, UK, ²Centre for Planetary Sciences, UCL/Birkbeck, London, UK, ³Now at Department of Physics and Astronomy, University of Southampton, Southampton, UK, ⁴Department of Atmospheric, Oceanic, and Space Sciences, University of Michigan, Ann Arbor, Michigan, USA, ⁵Department of Earth, Planetary, and Space Sciences, University of California, Los Angeles, California, USA, ⁶Department of Physics, Imperial College London, London, UK, ⁷Planetary Science Institute, Tucson, Arizona, USA, ⁸British Antarctic Survey, Cambridge, UK, ⁹Space Research Centre, University of Leicester, Leicester, UK, ¹⁰Now at Center for Space Physics, Boston University, Boston, Massachusetts, USA

Abstract We present a comprehensive study of the magnetic field and plasma signatures of reconnection events observed with the Cassini spacecraft during the tail orbits of 2006. We examine their “local” properties in terms of magnetic field reconfiguration and changing plasma flows. We also describe the “global” impact of reconnection in terms of the contribution to mass loss, flux closure, and large-scale tail structure. The signatures of 69 plasmoids, 17 traveling compression regions (TCRs), and 13 planetward moving structures have been found. The direction of motion is inferred from the sign of the change in the B_θ component of the magnetic field in the first instance and confirmed through plasma flow data where available. The plasmoids are interpreted as detached structures, observed by the spacecraft tailward of the reconnection site, and the TCRs are interpreted as the effects of the draping and compression of lobe magnetic field lines around passing plasmoids. We focus on the analysis and interpretation of the tailward moving (south-to-north field change) plasmoids and TCRs in this work, considering the planetward moving signatures only from the point of view of understanding the reconnection x -line position and recurrence rates. We discuss the location spread of the observations, showing that where spacecraft coverage is symmetric about midnight, reconnection signatures are observed more frequently on the dawn flank than on the dusk flank. We show an example of a chain of two plasmoids and two TCRs over 3 hours and suggest that such a scenario is associated with a single-reconnection event, ejecting multiple successive plasmoids. Plasma data reveal that one of these plasmoids contains H+ at lower energy and W+ at higher energy, consistent with an inner magnetospheric source, and the total flow speed inside the plasmoid is estimated with an upper limit of 170 km/s. We probe the interior structure of plasmoids and find that the vast majority of examples at Saturn show a localized decrease in field magnitude as the spacecraft passes through the structure. We take the trajectory of Cassini into account, as, during 2006, the spacecraft's largely equatorial position beneath the hinged current sheet meant that it rarely traversed the center of plasmoids. We present an innovative method of optimizing the window size for minimum variance analysis (MVA) and apply this MVA across several plasmoids to explore their interior morphology in more detail, finding that Saturn's tail contains both loop-like and flux rope-like plasmoids. We estimate the mass lost downtail through reconnection and suggest that the apparent imbalance between mass input and observed plasmoid ejection may mean that alternative mass loss methods contribute to balancing Saturn's mass budget. We also estimate the rate of magnetic flux closure in the tail and find that when open field line closure is active, it plays a very significant role in flux cycling at Saturn.

1. Introduction

Magnetic reconnection is a process by which stored energy can be explosively released and plasma trapped in separate magnetic domains can move from one region to the other and intermix. Magnetic reconnection can be sampled directly and indirectly by observing changes in the topology of the magnetic field near the reconnection site and by observing the products of reconnection such as magnetotail plasmoids. The reconnection between the interplanetary and planetary magnetic fields at the dayside magnetopause results

in the entry of some solar wind plasma, the escape of magnetospheric charged particles, and the transport of electromagnetic energy to the tail. Reconnection between the open magnetic field lines in the lobes of a magnetotail causes a reduction in the accumulation of open magnetic field flux [e.g., *Dungey*, 1961]. Reconnection can also occur between oppositely directed, closed magnetic field lines when they become strongly stretched. In that case, previously trapped plasma sheet material can be lost downtail into the solar wind [e.g., *Vasyliunas*, 1983]. Tail reconnection either of open or closed field lines drives sunward and antisunward flows, which carry mass and energy toward the dayside magnetosphere and down the tail. The plasma escaping down the tail as a result of reconnection is on magnetic field lines forming either quasi-closed magnetic loops, or “islands,” or helical magnetic fields called flux ropes [*Schindler*, 1974; *Hughes and Sibeck*, 1987; *Slavin et al.*, 1989; *Birn*, 1989]. Collectively, the plasma and magnetic flux making up these magnetic loops and flux ropes are termed “plasmoids” [*Hones*, 1976, 1977]. If a spacecraft directly encounters such structures, the primary signature as measured by a magnetometer will take the form of a deflection in the north-south component of the field, usually followed by unipolar northward or southward magnetic field depending upon the location of the spacecraft relative to the flux rope or loop and the x lines that created it (and on whether the background planetary field is northward, as at Earth, or southward, as at Jupiter/Saturn) [*Slavin et al.*, 2003a; *Eastwood et al.*, 2005; *Li et al.*, 2013]. The sense of the field deflection tells us which side of the reconnection x line the spacecraft is on at the time of observation. Tailward moving events at Saturn are expected to display a southward-to-northward turning of the field (opposite to the Earth due to the oppositely directed planetary dipole). As we describe later, many plasmoids at Saturn have an azimuthal/corotational component to their motion in addition to purely radial tailward motion. Plasmoids have larger north-south dimensions than the surrounding plasma sheet where they form, and this results in the lobe regions being compressed as the plasmoids move sunward or antisunward [*Slavin et al.*, 1984]. These “traveling compression regions” (TCRs) are readily observable in magnetic field measurements on the basis of the correlated compression in the total magnetic field and the north-south tilting of the draped magnetic field [*Slavin et al.*, 1993].

There are two important subcategories of plasmoid signature: flux ropes and loops. Loop-like plasmoids may be thought of as lossless “magnetic bottles” that transport plasma sheet plasma down the tail. In contrast, flux ropes are cylindrical magnetic structures of twisted flux tubes with a strong axial magnetic field, peaking in the center, which must connect either to the lobes of the tail or, if the plasmoid extends across the entire plasma sheet, to the interplanetary magnetic field (IMF) in the dawn and dusk magnetosheath. These subcategories of plasmoid structure are important, because they provide clues as to the large-scale structure of the tail prior to reconnection [e.g., *Eastwood and Kiehas*, 2014]. For example, at Earth, strong links have been found between the direction of the IMF B_y component, large-scale shear in the terrestrial magnetotail, and the formation of flux ropes there [e.g., *Moldwin and Hughes*, 1992]. In addition, plasmoids with a helical flux rope structure lose much of the plasma sheet plasma as they move, with large pitch angle ions and electrons being lost first. The plasmoid magnetic field can only relax toward its ultimate force-free configuration as the internal plasma is depleted and the low-beta, strong axial magnetic field region grows [e.g., *Hesse and Kivelson*, 1998]. Early studies at Earth [e.g., *Sibeck et al.*, 1984; *Moldwin and Hughes*, 1992] noted that most terrestrial plasmoids have a strong “core” field, characteristic of helical magnetic structures. Later studies went on to successfully model them as “force-free” (i.e., $J \times B = 0$) flux ropes, which represent the minimum energy state of the field [e.g., *Lepping et al.*, 1995]. This flux rope core field has since been shown to possess up to twice the intensity of the field in the tail lobes [*Slavin et al.*, 1995, 2003b]. Flux ropes have also been found in the solar wind [*Moldwin et al.*, 1995], the ionosphere and induced magnetotail of Venus [*Russell and Elphic*, 1979], and the magnetotail of Mars [*Eastwood et al.*, 2012]. Thus, it would seem that flux ropes are ubiquitous throughout the solar system. In section 4, we explore whether this is also true of Saturn’s magnetosphere.

Figure 1 shows a schematic representing the various magnetic field signatures that may arise from spacecraft traversals through or near plasmoids. Briefly, if the plasmoid is flux rope-like, we would expect to see a strong increase in the total field strength as the spacecraft passes through (or close to) the center of the structure. Loop-like plasmoids on the other hand could be identified by a decrease in the total field strength (which is zero in the exact center of the circular loop-like plasmoid; i.e., it is an O line). However, we note a strong caveat to this picture, i.e., that the field signature observed is strongly dependent on the trajectory of the spacecraft through the structure [*Slavin et al.*, 2003b; *Borg et al.*, 2012], as shown in the figure. We discuss

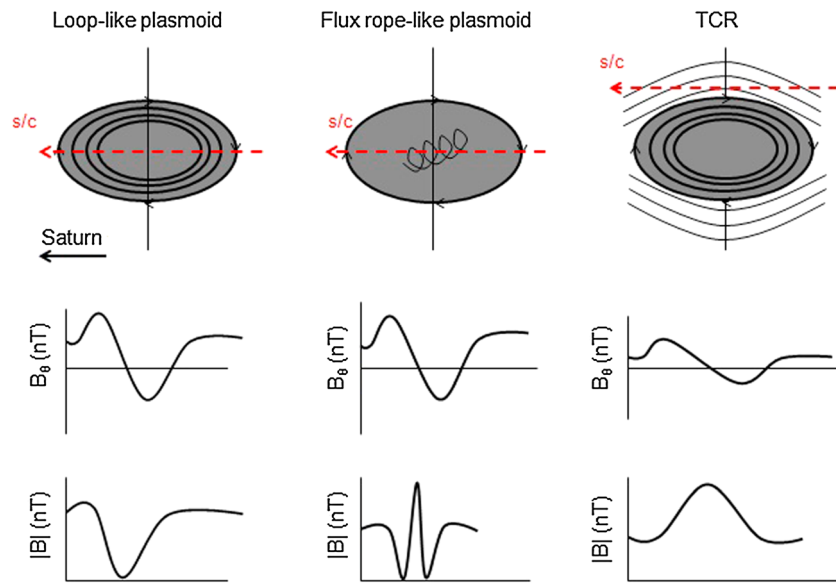


Figure 1. Schematic sketch of spacecraft trajectory through (a) tailward moving loop-like plasmoid, (b) tailward moving flux rope-like plasmoid, and (c) tailward moving TCR (adapted from Zong *et al.* [2004]).

the implications of this in more detail later (Figure 2). In addition to this, modeling of tail plasmoids by Kivelson and Khurana [1995] and observation of magnetopause flux transfer events by Zhang *et al.* [2010, 2012] indicated that it is possible for flux ropes to display a depressed field strength at their center due to the presence of a significant trapped hot plasma. We have not explored this possibility in this work due to a lack of continuous plasma data and/or multiple spacecraft passes.

The first in situ hint at reconnection in Saturn's magnetotail came on the outbound pass of Cassini's Saturn orbit insertion maneuver in 2004. Bunce *et al.* [2005], analyzing magnetic and plasma data, reported evidence of compression-induced tail reconnection accompanied by hot-plasma injection. The magnetometer signature at this time was consistent with a dipolarization of the field. Following on from this event, the best chance to search for evidence of reconnection came in 2006 with Cassini's tail orbit season. Jackman *et al.* [2007] analyzed the magnetometer data for three events, and that work was quickly followed by a presentation of plasma and energetic particle data for two of those events by Hill *et al.* [2008]. The events, interpreted as plasmoid passage, were characterized by small southward followed by sharp northward turnings of the field, representing tailward traveling structures, and estimates of the speed were on the order of ~ 800 km/s. The suggested location of the x line, estimated from plasma velocity data and energetic neutral atom (ENA) emission suggested to come from the reconnection site, was in the region of $\sim 26.5 R_S$ ($1 R_S = 60,268$ km), in line with previous estimates by Mitchell *et al.* [2005], who reported intense energetic neutral atom (ENA) fluxes emanating from this region. Later, Jackman *et al.* [2008a] added a further two events to the catalogue and showed energetic particle information depicting a change of the plasma flow from the corotation direction to a tailward direction with the passage of a plasmoid. Such deflection of the plasma flow from azimuthal to radial was also reported by McAndrews *et al.* [2009], who showed ion velocity flow measurements from the Cassini plasma spectrometer.

More recently, Jackman *et al.* [2011] examined the role of plasmoids in flux transport in Saturn's magnetosphere. They found evidence of a significant postplasmoid plasma sheet (PPPS), a region where open flux is being closed following the release of a plasmoid [Richardson *et al.*, 1987]. They estimated that the average PPPS interval at Saturn closes up to ~ 3 GWb of flux. From auroral images, it is estimated that Saturn's tail contains ~ 15 – 50 GWb of flux [e.g., Badman *et al.*, 2005, 2013], and thus, 3 GWb represents a significant fraction of this. While the calculation of the flux closed in the PPPS is sensitive to the assumptions about the azimuthal extent of plasmoids, the estimates agree very well with the results of the global MHD simulation of Jia *et al.* [2012], who estimated 3.5 GWb of flux closure from a typical reconnection event at Saturn.

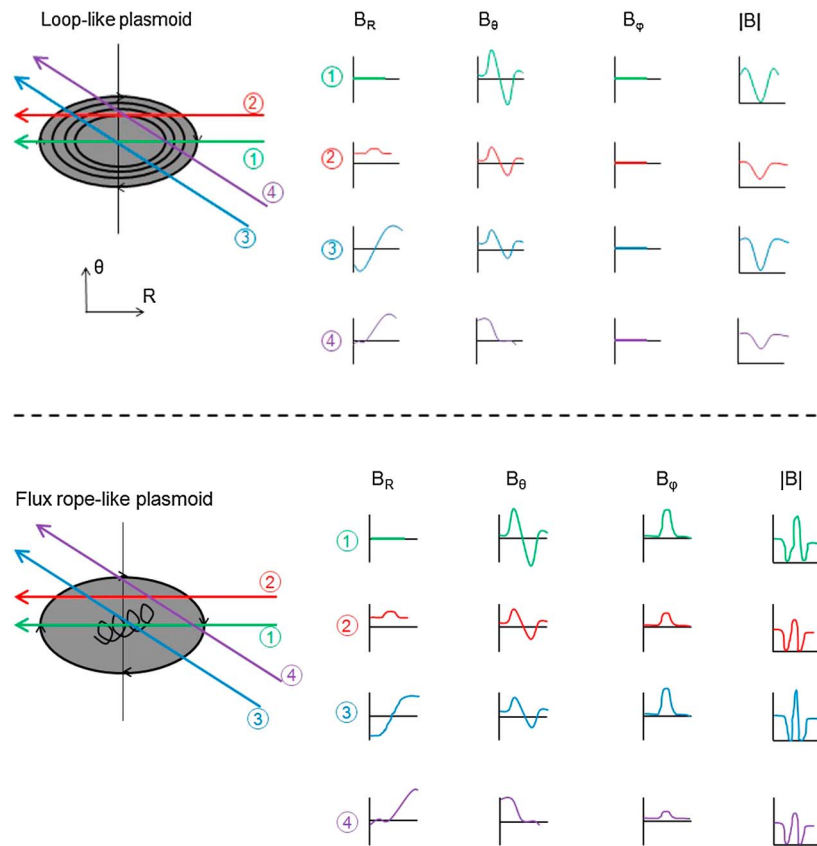


Figure 2. Schematic of various possible spacecraft trajectories through model tailward moving loop-like and flux rope-like plasmoids and the field signatures (in KRTP coordinates) that would result. B_R is positive above the current sheet, B_θ is positive southward, and B_ϕ is positive in the corotation direction. The various straight line trajectories assume that the encounters occur in a short time scale compared with the times for dynamical changes of the local magnetosphere. (After Borg et al. [2012]).

The aim of this paper is to provide a new comprehensive survey of reconnection signatures in Saturn’s magnetotail, primarily from the perspective of the Cassini magnetometer data but with the addition of plasma data where appropriate. Since the first observation of a planetward moving dipolarization [Bunce et al., 2005] and tailward moving plasmoids [Jackman et al., 2007], many questions have arisen regarding the local properties of the reconnection region (such as magnetic field reconfiguration and plasma flow changes) and the global impact of reconnection in terms of its role as a flux closure and mass removal method. We show the statistics of the location of reconnection events and describe the size and properties of plasmoids and TCRs. For the first time, we probe the interior structure of plasmoids at Saturn to determine the nature of the magnetic fields inside them. We compare and contrast our observations with those in other planetary magnetotails and look to the future of exploration of Saturn’s magnetotail. In section 2, we introduce the data set used in our study. Section 3 includes several case study examples of reconnection events, as well as superposed epoch analyses showing the average field profiles for reconnection signatures. Section 4 investigates the interior structure of plasmoids, section 5 provides a general discussion, and section 6 summarizes our key results.

2. Data Set and Observations

As introduced above, reconnection events can be identified by changes in the north-south component of the magnetic field. We have surveyed the data from the Cassini magnetometer [Dougherty et al., 2004] in Saturn’s tail during 2006, the period where Cassini executed its deepest orbits of the tail, providing us with some of the best chances to observe the products of reconnection. The coordinate system used throughout this

paper is the kronocentric radial theta phi (KRTP) system, where the radial component (B_r) is positive outward from Saturn, the theta component (B_θ) is positive southward, and the azimuthal component (B_ϕ) is positive in the direction of planetary corotation. *Jackman et al.* [2009] discussed the merits of this coordinate system in detail, particularly emphasizing how it can help to differentiate between plasmoid passage and a wavy current sheet. This is a Saturn-centric coordinate system, and *Jackman and Arridge* [2011] showed that the average B_θ component is small and positive (southward) in the tail during 2006. We are seeking departures from this “steady state” behavior, and thus, we began by defining a background for the B_θ component by taking a running average of 1 min resolution data over 1 day, similar to the method employed by *Vogt et al.* [2010] for Jupiter. From this point, we selected a subset of events for further examination, where the magnitude of the B_θ component was close to or above background levels and the spacecraft was beyond $15 R_S$ on the nightside. We then selected by eye those events which exhibited clear, unambiguous field deflections. We additionally required that the B_θ component cross through zero at some point during the event. The start and end of the event were assigned as the local south/north extrema in B_θ . The sign of the change in B_θ indicates whether the spacecraft was tailward or planetward of the reconnection x line. As mentioned in the introduction above, when looking for tailward moving plasmoids or TCRs, we expect a southward-to-northward turning of the field, as evidenced by a positive-to-negative change in B_θ and vice versa for planetward moving events.

We used two key methods to differentiate plasmoids from TCRs. First, we inspected the magnetic field components. Both plasmoids and TCRs yield a change in the B_θ component, although the amplitude of this change (determined from the local extrema in the north-south component around the central turning) is expected to be smaller for TCRs than plasmoids (as illustrated in Figure 1). TCRs also display a very characteristic signature in terms of the total field strength. As illustrated in Figure 1, the smooth tilting in B , associated with the wrapping of lobe field lines around passing plasmoids, is the key feature which distinguishes TCRs from plasmoids. Flux ropes also feature an increase in the field magnitude, but for a flux rope, this increase is very abrupt and is due primarily to the axial field, while the TCR signature is more gradual and lacks a strong axial field. Second, we took the spacecraft position into account to understand whether the spacecraft was in the lobes or plasma sheet when observing passing structures. Here the sign and magnitude of the radial field component can provide clues as to whether the spacecraft is close to the current sheet or is farther out in the lobes. Additionally, we have supported our analysis with a detailed inspection of data from the Cassini plasma spectrometer (CAPS), electron spectrometer (ELS), and ion mass spectrometer (IMS) instruments, where electron and ion populations in the lobes and plasma sheet show characteristic differences. If the spacecraft is deep in the lobes, we expect to see TCRs rather than plasmoids.

Through our search, we found a total of 69 south-north signatures, which we interpret as tailward moving plasmoids; 17 TCRs (15 tailward and 2 planetward); and 13 north-south signatures, which we interpret as planetward moving structures. The “tailward” and “planetward” motion is inferred from the sign of the change in B_θ . When the CAPS instrument look direction was favorable, we also inspected the plasma flows, and indeed in the vast majority of plasmoid cases (29/35 for which a flow direction, if not a flow velocity, could be inferred), there was some tailward component to the flow. However, it was also common for a significant component of the flow to be in the corotation/azimuthal direction. Nonetheless, for simplicity, we refer to plasmoids with a south-north field signature as “tailward moving” for the remainder of this paper. There was a single example (2006 day 261 04:01), where the field displayed a north-south-north turning and the plasma data indicate an inward flow. We have still classed this example as a plasmoid, because the south-north turning of the field was dominant (as selected by our automated technique), but such an example warrants further study and may shed light on the existence of multiple reconnection sites in Saturn’s tail, which may yield such a combination of field and flow signatures. On average, the amplitude of plasmoids ranged from ~ 0.61 to 4.2 nT and the amplitude of the TCRs from ~ 0.12 to 2.22 nT. All 69 plasmoids had a value of B_θ that exceeded the background during the event, and 66/69 events had B_θ that exceeded $1.5 \times$ the background. Because we placed minimum requirements on the field change associated with our events, it is possible that there are many smaller-amplitude events in the data that we have not included in our list. Thus, our list represents a select set of robust events that may represent a lower limit on the occurrence rate of reconnection in Saturn’s tail.

Plasmoid signatures can be somewhat more complicated than TCRs. Sophisticated modeling [e.g., *Slavin et al.*, 2003a] and multispacecraft data analysis at Earth [e.g., *Borg et al.*, 2012; *Henderson et al.*, 2006] have revealed the complex topology of the tail post-reconnection and the sensitivity of magnetic field traces to

Table 1. Timings and Properties of Plasmoids and TCRs Observed During 2006

Type	Day of Year	Time (h: min: s)	Start Time (h: min: s)	End Time (h: min: s)	Range (R _S)	LT (h: min)	Duration (min)	ΔB_{θ} (nT)	B_{θ} Change	Classification	Plasma Flow Velocities ^a	Ion Flow Direction
Plasmoid	32	12:58:00	12:47:00	13:11:00	65.99	4:26	24.00	2.13	south-north	isolated	V (W+)~200-270 km/s	strongly outward
TCR	36	04:32:00	04:17:00	04:38:00	68.17	4:46	21.00	0.52	south-north	pair		
Plasmoid	36	05:41:00	05:34:00	06:02:00	68.17	4:46	28.00	0.63	south-north	pair		
Plasmoid	37	23:10:30	23:02:30	23:20:30	68.08	4:56	18.00	0.87	south-north	isolated	CAPS data gap	CAPS data gap
Plasmoid	60	07:33:00	07:30:20	07:36:00	32.33	2:17	5.67	2.16	south-north	multiple	V (W+)~170 km/s	corotation and outward
Plasmoid	60	08:27:00	08:25:30	08:28:00	32.50	2:17	2.00	0.94	south-north	multiple		
TCR	60	08:58:00	08:53:00	09:03:00	32.61	2:18	10.00	0.49	south-north	multiple		
TCR	60	09:34:00	09:33:00	09:36:00	32.71	2:18	3.00	0.12	south-north	multiple		
TCR	62	15:26:00	15:19:00	15:30:00	40.93	2:55	11	0.31	south-north	pair		
TCR	62	16:33:00	16:29:00	16:38:00	41.07	2:56	9.00	0.22	south-north	pair		
Plasmoid	63	22:07:00	22:06:00	22:09:00	44.10	3:10	3.00	1.70	south-north	pair	V(W+)~200 km/s	halfway between corotation and outward
Plasmoid	63	22:59:30	22:56:00	23:02:00	44.17	3:11	6	3.51	south-north	pair	V (W+)~580 km/s V (H+)~620 km/s	outward, from above, and slightly westward
Plasmoid	64	08:50:00	08:48:00	08:54:00	44.98	3:15	6.00	0.90	south-north	multiple	V (W+)~220 km/s	outward
Plasmoid	64	09:30:45	09:29:00	09:32:20	45.03	3:15	3.33	1.01	south-north	multiple	V (W+)~290 km/s	strongly outward
Plasmoid	64	10:49:00	10:46:10	10:52:10	45.13	3:16	6.00	1.15	south-north	multiple	V (W+)~220 km/s	strongly outward
Plasmoid	64	19:56:30	19:49:00	20:04:00	45.78	3:20	15.00	1.19	south-north	isolated		
Plasmoid	65	06:34:00	06:28:00	06:39:00	46.45	3:24	11.00	0.78	south-north	isolated		
Plasmoid	65	17:03:00	17:00:45	17:05:00	47.00	3:29	4.25	0.61	south-north	pair		
Plasmoid	65	17:24:00	17:22:00	17:27:15	47.02	3:29	5.25	1.31	south-north	pair		
Plasmoid	65	21:08:00	20:59:00	21:17:00	47.20	3:30	18.00	0.97	south-north	isolated		
TCR	66	06:23:00	06:17:00	06:30:00	47.6	3:36	13	0.6	south-north	pair		
TCR	66	08:42:00	08:40:00	08:51:00	47.7	3:36	11	0.7	south-north	pair		
TCR	83	18:34:30	18:18:30	18:46:00	34.03	0:33	27.50	2.22	south-north	isolated		
Plasmoid	84	02:31:30	02:30:30	02:32:30	35.8	0:7	2	1.9	south-north	isolated	outward: V (W+)~245 km/s	outward
Plasmoid	85	00:16:00	00:09:00	00:20:00	40.22	0:58	11.00	1.85	south-north	isolated		outward
TCR	85	04:20:00	04:01:00	04:25:00	40.9	1:0	24	0.6	south-north	isolated		
TCR	124	08:33:00	08:32:00	08:42:00	38.40	0:43	10.00	0.62	south-north	isolated		
TCR	124	13:13:00	13:05:00	13:20:00	39.05	0:45	15.00	0.20	north-south	pair		
TCR	124	14:19:30	14:06:00	14:30:00	39.20	0:46	24.00	0.65	north-south	pair		
Plasmoid	131	13:55:00	13:40:30	14:16:30	48.28	2:01	36.00	1.35	south-north	isolated		progression from eastward to radial outward to westward flow
TCR	131	22:48:00	22:19:00	22:57:00	48.09	2:05	38	0.84	south-north	isolated		
TCR	169	00:34:00	00:32:00	00:39:00	62.32	1:34	7.00	1.47	south-north	isolated	V (H+)~620 km/s	outward
Plasmoid	193	07:28:30	07:27:00	07:43:00	48.42	23:52	16	2.1	south-north	isolated	V (W+)~1240 km/s V (H+)~679 km/s	strongly outward and slightly westward (field aligned)
Plasmoid	195	01:48:00	01:42:00	02:05:00	47.61	0:09	23.00	2.22	south-north	Pair		
TCR	195	04:08:00	04:07:00	04:13:00	47.52	0:10	6.00	0.38	south-north	Pair		
TCR	195	12:44:00	12:38:00	12:53:00	47.16	0:13	15	0.69	south-north	isolated		
Plasmoid	195	23:38:30	23:31:00	23:45:00	46.5	0:3	14	1.6	south-north	isolated		
Plasmoid	196	08:56:00	08:54:00	09:01:00	46.05	0:22	7.00	1.15	south-north	Pair	V (W+)~202 km/s	strongly outward
Plasmoid	196	10:22:00	10:15:00	10:24:00	45.96	0:23	9.00	1.40	south-north	Pair	V (W+)~202 km/s	outward
Plasmoid	196	18:22:00	18:24:00	18:30:00	45.41	0:26	6.00	1.25	south-north	isolated	V (W+)~186 km/s	slightly outward
Plasmoid	197	07:09:00	07:05:00	07:12:00	44.41	0:32	7.00	1.60	south-north	Pair		
TCR	197	07:44:00	07:40:00	07:51:00	44.36	0:32	11.00	0.38	south-north	Pair		
Plasmoid	197	16:34:00	16:25:00	16:41:00	43.5	0:6	16	0.9	south-north	isolated	V (W+)~170 km/s	outward
Plasmoid	198	14:45:30	14:43:30	14:52:30	41.25	0:48	9.00	1.75	south-north	isolated		
Plasmoid	199	23:06:45	23:02:00	23:08:30	36.88	1:08	6.5	1.80	south-north	isolated		

Table 1. (continued)

Type	Day of Year	Time (h: min: s)	Start Time (h: min: s)	End Time (h: min: s)	Range (R_S)	LT (h: min)	Duration (min)	ΔB_{θ} (nT)	B_{θ} Change	Classification	Plasma Flow Velocities ^a	Ion Flow Direction
Plasmoid	209	20:34:00	20:17:00	20:38:30	36.85	22:24	21.50	2.58	south-north	isolated		
Plasmoid	212	04:49:00	04:39:00	04:57:00	43.85	22:56	18.00	0.84	south-north	Pair		corotation
Plasmoid	212	05:27:00	05:15:00	05:57:00	43.91	22:56	42.00	0.65	south-north	Pair		corotation
Plasmoid	212	10:07:00	10:05:00	10:08:00	44.34	22:58	3.00	0.68	south-north	Pair		uncertain direction; spacecraft rolling but CAPS not looking in corotation direction
Plasmoid	212	10:54:00	10:48:00	10:58:00	44.41	22:36	10.00	1.08	south-north	Pair		
Plasmoid	212	14:57:00	14:50:00	15:00:00	44.76	23:00	10.00	0.91	south-north	isolated		
Plasmoid	212	23:19:30	23:17:30	23:20:30	45.4	23:1	3	1.1	south-north	isolated		
Plasmoid	213	11:50:00	11:32:00	12:12:00	46.4	23:2	40	1.5	south-north	isolated		
Plasmoid	214	18:32:00	18:29:00	18:35:00	48	23:4	6	0.8	south-north	isolated		
Plasmoid	215	10:36:30	10:30:00	10:38:30	48.5	23:5	8.5	1.1	south-north	isolated		
Plasmoid	215	17:27:00	17:20:00	17:35:00	48.7	23:31	15.0	0.83	south-north	isolated		outward
Plasmoid	216	16:47:30	16:45:00	16:51:15	49.00	23:41	6.25	3.39	south-north	Pair		strongly outward
Plasmoid	216	17:51:00	17:47:30	17:55:30	49.01	23:50	8	0.82	south-north	Pair		
Plasmoid	217	17:42:00	17:28:20	17:59:00	48.85	23:13	21.67	0.65	south-north	isolated		corotation or very slightly outward
Plasmoid	218	15:27:00	14:47:00	16:05:00	48.31	23:59	78.00	0.92	south-north	isolated		
Plasmoid	219	11:20:00	10:45:00	12:20:00	47.48	00:07	95.00	1.03	south-north	isolated		
Plasmoid	223	14:40:00	14:26:00	15:07:00	37.99	00:56	41.00	1.21	south-north	isolated		very weak ions, apparently outward
Plasmoid	232	10:01:00	09:46:00	10:07:00	30.76	21:54	21.00	1.91	south-north	isolated		very weak ions, uncertain flow direction
Plasmoid	234	14:50:30	14:45:00	15:03:00	39.6	22:6	18	1.8	south-north	isolated		no discernible ion flow
Plasmoid	236	18:05:30	18:04:30	18:11:00	45	23	6.5	0.95	south-north	Pair		
Plasmoid	238	18:16:00	18:15:00	18:18:30	47.9	23:3	3.5	1.3	south-north	isolated		outward
Plasmoid	240	00:41:00	00:33:00	00:44:00	48.73	23:32	11.00	1.20	south-north	isolated		
Plasmoid	240	06:48:00	06:46:00	06:55:00	48.81	23:34	9.00	0.66	south-north	isolated		initially, flow outward and from above; subsequently, largely corotating
Plasmoid	240	23:38:30	23:28:00	23:54:00	48.8	23:6	26	1.5	south-north	multiple		outward
Plasmoid	241	01:38:30	01:34:30	01:53:30	48.8	23:6	20	1.1	south-north	multiple		
Plasmoid	241	03:40:30	03:25:00	03:45:00	48.8	23:7	5	0.55	south-north	multiple		
Plasmoid	242	17:30:00	17:02:00	17:50:00	48.02	23:57	48.0	0.98	south-north	isolated		uncertain flow direction (probably corotational)
Plasmoid	243	09:05:00	08:52:00	09:10:00	47.3	0:1	18	1.4	south-north	isolated		
Plasmoid	243	21:47:00	21:22:00	21:58:00	46.64	00:09	36.00	0.64	south-north	isolated		outward flowing H+ precedes event, which coincides with departure from electron plasma sheet
Plasmoid	244	15:17:00	15:11:00	15:19:00	45.45	00:16	8.00	1.15	south-north	isolated		
Plasmoid	246	22:45:00	22:18:00	22:51:00	39.74	00:45	33.00	2.02	south-north	isolated		viewing away from corotation, but clearly outward
Plasmoid	248	17:50:00	17:45:00	18:00:00	32.8	1:3	15	1.6	south-north	Pair		probably outward
Plasmoid	248	18:30:00	18:29:00	18:31:00	32.8	1:3	2	1.4	south-north	Pair		outward
Plasmoid	249	12:04:00	12:02:30	12:04:30	29.14	01:34	2.00	2.00	south-north	Pair		slightly outward on both sides of event
Plasmoid	249	15:34:00	15:32:15	15:36:45	28.35	1:38	4.50	4.42	south-north	isolated		outward

Table 1. (continued)

Type	Day of Year	Time (h: min: s)	Start Time (h: min: s)	End Time (h: min: s)	Range (R_S)	LT (h: min)	Duration (min)	ΔB_θ (nT)	B_θ Change	Classification	Plasma Flow Velocities ^a	Ion Flow Direction
Plasmoid	250	00:32:30	00:11:30	00:33:45	26.22	01:49	22.25	2.25	south-north	isolated		uncertain flow direction (not actuating) flow from above (inward/outward uncertain)
Plasmoid	258	10:05:00	09:20:00	10:10:00	35.4	23.9	50	2.2	south-north	isolated	V (W+) ~480 km/s	
Plasmoid	258	21:00:00	20:20:00	21:20:00	36.2	0	60	2.1	south-north	isolated		
Plasmoid	261	04:01:00	03:58:30	04:05:45	37.52	00:31	7.25	1.66	south-north	isolated	V(W+) > 600 km/s	inward?
Plasmoid	262	08:45:00	08:30:30	08:49:00	36.54	00:47	18.50	1.10	south-north	isolated	V(W+) ~220 km/s	corotation
Plasmoid	264	02:08:30	02:00:30	02:09:30	32.99	01:12	9.00	1.59	south-north	isolated		

^aFlow speeds are estimated from the energy of the peak counts, and thus, they represent upper limits.

the trajectory through plasmoids. Figure 2 illustrates some example trajectories through model flux ropes and loop-like plasmoids, along with the corresponding expected magnetic field signatures. While a bipolar south-north change in B_θ (of varying amplitude) is common to nearly every encounter with a tailward moving plasmoid, the sense, magnitude, and duration of the changes in the radial and azimuthal field components and field magnitude are highly sensitive to the spacecraft trajectory through the structures. The B_ϕ component in particular is significantly different for loops and flux ropes.

The date, time, and properties of the plasmoids and TCRs are provided in Table 1. We have listed the duration and peak-to-peak amplitude of all events. The duration is defined as the interval between the local maximum positive (southward) and negative (northward) excursions in the B_θ component. We note (see Figure 5c) that the duration as defined from the magnetic field signature can be shorter than the duration as inferred from the plasma data, and according to the force-free flux rope model of Kivelson and Khurana [1995], our definition may underestimate the plasmoid size by a factor of ~4–8. We note also that occasionally, the endpoints of the signatures can be uncertain due to either the presence of multiple local maxima or minima in B_θ or very broad extrema that smoothly blend into the background tail field. However, this method of defining the duration by the peak northward/southward excursions gives a consistent and reproducible measure of these structures and has also been used in the analysis of plasmoids at Jupiter [Vogt et al., 2014]. The amplitude is the total peak-to-trough amplitude in the B_θ perturbation. Events were also classified in terms of whether they were observed in isolation, or in pairs or groups, following the classification employed by Slavin et al. [1993] (hereafter S93) for the terrestrial tail. “Isolated” events were those observed to be separated from other events by at least 180 min. “Paired” events were defined as those separated by less than 180 min, while “multiple” events were those in which several TCRs or plasmoids were observed without a gap of more than 180 min between successive events. We note that this 180 min time scale is much longer than the analogous 30 min time scale employed by S93. This reflects the larger system size and inherently longer time scales for plasma circulation and reconnection processes at Saturn compared to Earth. The vast majority of events were observed in isolation. It is impossible to say with a single spacecraft whether most reconnection events result in the release of a single plasmoid, or whether they release many which may, for one reason or another, be missed by the spacecraft if they travel in relatively narrow channels downtail. We do however study the paired and multiple events with particular interest, such as the series of three plasmoids on day 64 that Jackman et al. [2011] analyzed and the series of four closely spaced events on day 60 described in section 3.1.

We incorporate both the tailward and planetward moving events in this section, as the full sample helps toward our understanding of reconnection recurrence. However, we focus only on tailward moving plasmoids and TCRs for the subsequent sections. We leave

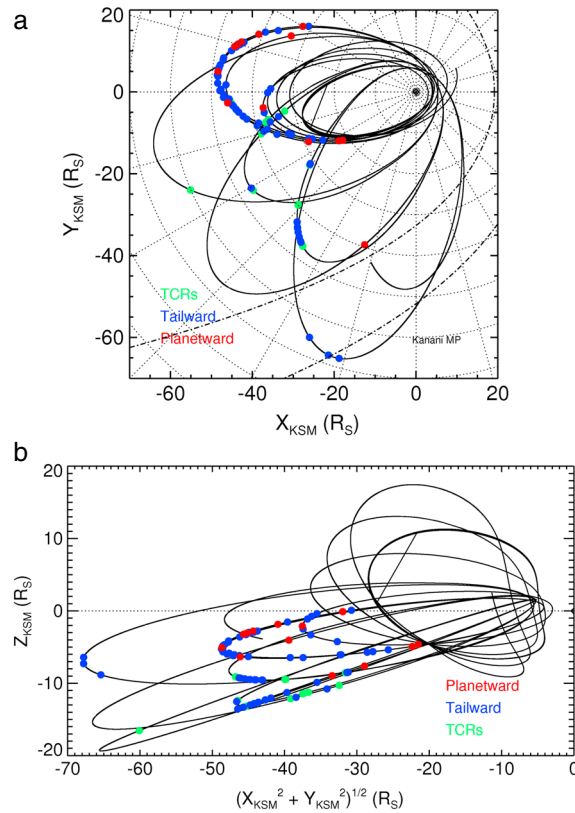


Figure 3. Cassini trajectory for 2006 day 18–291 in the kronocentric solar magnetospheric (KSM) coordinate system. KSM is the kronian analogue of GSM, where the x axis coincides with the direction to the Sun, the x - z plane contains the planetary dipole axis, and the y component is azimuthal, positive toward dusk. The blue, red, and green dots show the location of the tailward and planetward moving structures and TCRs, respectively. (a) The x - y KSM view. The Kanani *et al.* [2010] model magnetopause is overplotted for the solar wind dynamic pressures of 0.1 and 0.01 nPa. (b) The ρ - z KSM view.

Jupiter, for example, we might have expected with a large statistical sample to see a clear separatrix between tailward moving and planetward moving events. This in turn could indicate the average position of the tail reconnection x line. However, in our case, there is no such clear demarcation. This may indicate that the reconnection x -line position at Saturn is highly sensitive to magnetospheric conditions. For example, it could be strongly linked to the effect of solar wind compression changing the size of the magnetospheric cavity. The recent modeling work of Jia *et al.* [2012] indicates that the x line can be present anywhere between ~ 25 and $40 R_S$. Their model indicated that for cases when the Dungey cycle is active, reconnection occurs closest to the planet under the conditions of strong solar wind compression and further from the planet under expanded magnetospheric conditions.

Figure 3b illustrates the latitudinal coverage of the spacecraft. The trajectory during 2006 was such that most of the orbits at the start of the interval were in the equatorial plane toward the dawn flank, with the spacecraft only reaching higher latitudes later in the year. The observation of plasmoids and TCRs is highly latitude dependent. TCRs are observed at latitudes ranging from -0.03° to $+0.44^\circ$, while plasmoids are observed at latitudes ranging from -0.43° to $+15.2^\circ$. We must interpret this latitude spread in the context of the southern hemisphere summer conditions during 2006, where low latitudes tended to correspond to southern lobe and higher positive latitudes corresponded to the nominal hinged current sheet position (where plasmoids form). We note the strong bias toward plasmoid observation after day 200 of 2006, when

the analysis and interpretation of events planetward of the x line to future work as their properties and their ultimate fate as they travel toward the inner magnetosphere warrant a separate and much more detailed discussion.

The locations of all the events superimposed on the Cassini's trajectory during 2006 are shown in Figures 3a and 3b. As can be seen from Figure 3a, a view of the equatorial plane from the north, Cassini's trajectory over this interval was largely biased toward dawn, with the deepest tail passes occurring postmidnight. We note from Figure 3a that tailward moving plasmoids are observed at all local times, where there is spacecraft coverage. A striking point from Figure 3a is that there is no clear division in radial distance between the tailward and planetward observations, other than to say that planetward moving events are observed within $\sim 50 R_S$. By analogy with Earth, where a near-planet x line might be $\sim 30 R_E$ downtail [Imber *et al.*, 2011], and a distant x line might be $\sim 100 R_E$ downtail [Slavin *et al.*, 1985], we can scale this (based on the average magnetopause standoff distances at Earth and Saturn of $10 R_E$ and $25 R_S$, respectively) to an expected near-planet x -line distance of $\sim 75 R_S$ and expected distant x -line distance of $\sim 250 R_S$ at Saturn. The latter estimate is far beyond the maximum downtail distance of $68 R_S$ reached by Cassini in 2006. We interpret all of the examples in this work as linked to reconnection processes local to a near-Saturn x line, which we infer from our observations to be typically significantly closer to the planet than the scaled estimate of $75 R_S$. Based on the work of Vogt *et al.* [2010] at

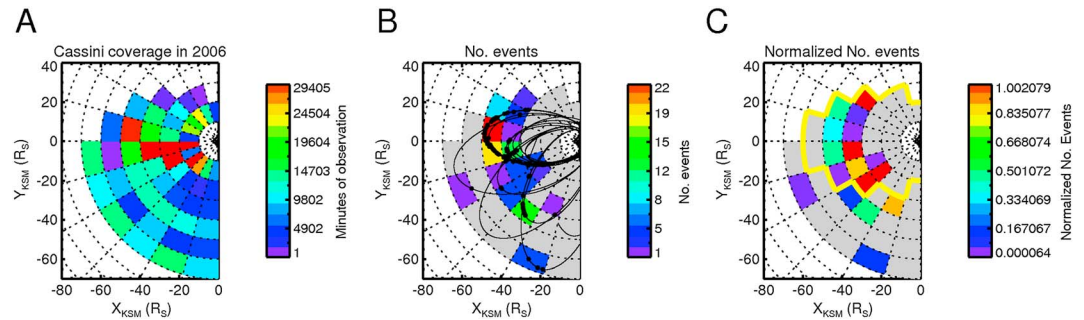


Figure 4. Color-coded plots of Saturn’s nightside showing the properties of particular radial distance and local time sectors. All the plots are equatorial plane views with the Sun to the right. In all panels, the white represents the bins with no spacecraft coverage, and the grey represents the bins with trajectory coverage but no reconnection events. (a) The number of minutes the Cassini spacecraft spent on the nightside during 2006, in the bins of 10 R_S in radial distance by 1 h in local time. (b) The number of reconnection events seen in each sector by Cassini. The spacecraft trajectory during 2006 is overlaid, as are the black points to illustrate the precise locations of tailward moving plasmoids, TCRs, and planetward moving events. (c) The number of reconnection events normalized to observation time. The thick yellow lines surround the bins symmetric either side of midnight, where there was spacecraft coverage.

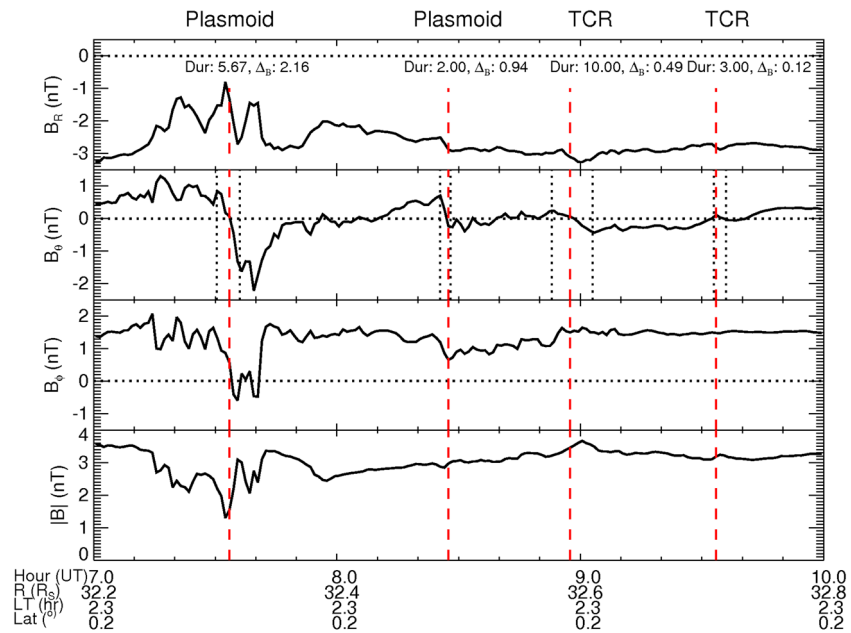
the Cassini orbits began to move out of the equatorial plane to higher latitudes. No TCRs were observed beyond day 197 of 2006.

Knowing that reconnection observations are highly trajectory dependent, it is important to understand not only the nature of the spacecraft trajectory but also how the events are distributed, such that we can search for specific occurrence trends. Figure 4a shows the amount of the time that the spacecraft spent in different range and local time sectors, Figure 4b shows the spread of events, and Figure 4c shows the number of events normalized to the exploration time. Figure 4a illustrates that most coverage was in the postmidnight sector inside of 40 R_S , with reasonably concentrated coverage just premidnight and postmidnight. This figure again illustrates the disparity of observation between dusk and dawn. Figure 4b shows the distribution of the events themselves. Grey bins indicate regions where Cassini flew through without observing any reconnection events. A clustering of events is observed around midnight in the range of 30–50 R_S . There is another noteworthy active region between 40–50 R_S and 03–04 LT. Figure 4c allows us to join the information from Figures 4a and 4b. It shows the occurrence of reconnection events normalized by the time spent by the spacecraft in each spatial bin. This is key because it helps us to understand whether the distribution of our events is due to an observational bias or to a genuine increased likelihood of reconnection in particular portions of Saturn’s tail. Thick yellow lines surround the regions premidnight and postmidnight, where there has been relatively symmetric coverage by the Cassini spacecraft. Within these regions, there is a significantly greater incidence of observation of reconnection postmidnight than premidnight; i.e., the likelihood of observing reconnection increases with local time throughout this region. The implications of this are discussed in section 5.

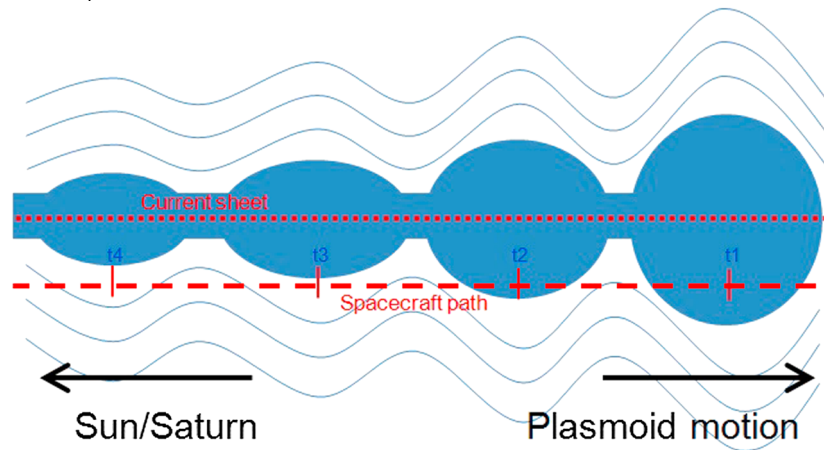
3. Individual and Averaged Field Signatures

3.1. Chain of Plasmoids and TCRs: 2006 Day 60 (1 March)

Examples of isolated plasmoids and TCRs in Cassini magnetometer data have been shown in several papers as detailed in the introduction [e.g., Jackman *et al.*, 2007, 2008a]. More recently, a “chain” of three plasmoids was observed [Jackman *et al.*, 2011] over 3 h, and it was suggested that these were formed either as a result of episodic reconnection events closely spaced in time or simultaneous reconnection at multiple, closely spaced x lines. In Figure 5a, we now show another example of a chain of events. The interval is 2006 day 60 07:00–10:00, during which Cassini observed two plasmoids and two TCRs. The panels in Figure 5a display the field in KRTP coordinates as defined above. This system allows us to clearly identify reconnection events, primarily through changes in the north-south (B_θ) component. In addition, the radial and azimuthal components can be used to elucidate the degree of corotation of the plasma (i.e., whether we are observing lagging or leading field lines).



a)



b)

Figure 5. (a) Cassini magnetic field data in KRTP coordinates for 2006 day 60 07:00–10:00. The positions of two plasmoids and two TCRs are marked with vertical lines, and the amplitude and duration in minutes of the signatures are listed in the first panel. (b) Schematic of expected geometry of the magnetotail during the passage of the plasmoids and TCRs. (c) Plasma and magnetic field observations for two plasmoids and two TCRs identified on 1 March 2006. The fourth panel reproduces the magnetic field measurements in Figure 6a, while the second and third panels above show the color-coded count rate in the CAPS ion mass spectrometer (above) and electron spectrometer (below) as a function of energy and time through the event. The black dashed boxes surround the intervals defined as the “duration” of the events from Figure 6a. The top row shows the all-sky images of the ion distribution at 2.4 keV (first two) and 4.1 keV (third). In this format, the look direction toward Saturn is in the center. The radial distance from the center is proportional to the polar angle of the viewing direction relative to Saturn’s direction. Thus, the entire outer circle corresponds to the anti-Saturnward look direction, and the dashed circle halfway to the outer boundary indicates look directions that are 90° away from Saturn’s direction. The azimuth in the plots (indicated by the angle markings around the circumference of the outer circle, given in degrees) corresponds to the azimuth of the look direction relative to a meridian containing the direction to Saturn and Saturn’s spin (and magnetic dipole) axis, measured about the axis pointing toward Saturn. Thus, the corotation look direction (indicated by the filled triangle) lies at a polar angle of 90° and an azimuthal angle of 270°. Particles coming from the direction of Saturn are seen at look directions interior to the dashed 90° circle, and particles flowing toward Saturn are seen at look directions exterior to that circle.

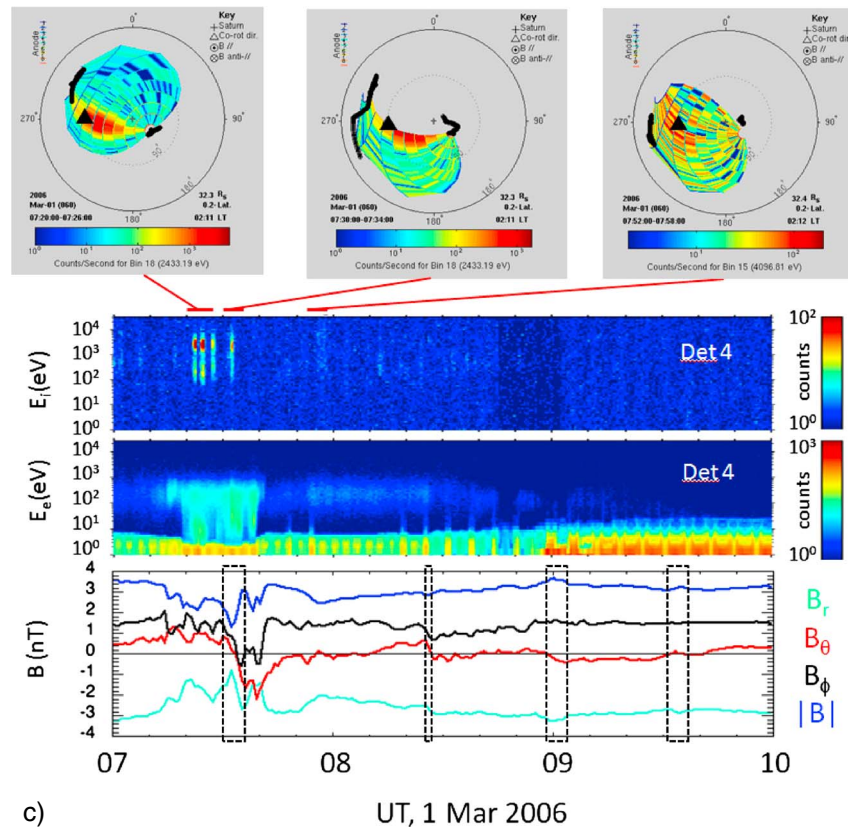


Figure 5. (continued)

The timings of the plasmoids and TCRs are marked in Figure 5a by vertical dashed lines. The duration of the events and their total ΔB_θ are listed in the first panel. As explained above, the duration is defined as the time between the local southward and northward extrema in the B_θ component either side of the central field deflection. The first of the plasmoids at $\sim 07:32$ displays the largest field deflection of 2.16 nT. The duration of the signature based on the southward and northward field extrema is ~ 5 min, but we note the extended interval of northward field after the plasmoid passage. The plasma data for this signature are presented in Figure 5c and discussed below. The next plasmoid signature is much smaller, with only a 0.94 nT deflection but again the same sense of northward turning of the field. Following on from this, there are two TCRs within 45 min of one another, evidenced by the northward turnings of the field and the small localized compressions in the field magnitude. The second TCR has a very small amplitude change in B_θ (0.12 nT), but does display the smooth tilting of the magnetic field characteristic of TCRs. The first plasmoid is seen by the spacecraft at a radial distance of $32.33 R_S$, and from inspection of the sign of the field change, we infer that Cassini was tailward of its source, observing the structure propagate down the tail. The same holds for the other three events. We suggest that all of these observations are linked to a common reconnection episode which produced multiple plasmoids.

With a single spacecraft, we are unable to separate temporal from spatial effects, but we can suggest two plausible scenarios which could result in this multi-event observation. In the first scenario, the reconnection episode results in the release of four plasmoids, whose effects are observed sequentially as illustrated in Figure 5b (similar to a terrestrial morphology suggested by Slavin *et al.* [1993, 2005]). In this case, Cassini (which was sampling the tail at approximately constant latitude during this interval) penetrated relatively deep into the center of the first, largest plasmoid (decrease in $|B|$ to ~ 1.4 nT, where $|B| = 0$ would represent the center of a perfectly loop-like plasmoid). We then suggest that the second plasmoid was smaller, and so the spacecraft only caught the edge of it. This interpretation is borne out by the smaller northward turning and the smaller decrease in $|B|$. The vertical extent of the third and fourth plasmoids was such that they did

not encompass the spacecraft track at all. Rather, we suggest that Cassini passed through the compressed lobe field lines draped around the passing plasmoid structures and observed TCR signatures of decreasing amplitude. Again, this tendency for the amplitude of TCRs, and by implication the north-south extent of plasmoids, to decrease from one TCR to the next in chain events is frequently observed at Earth [Slavin *et al.*, 1984, 1993, 2005]. A second plausible scenario also involves the ejections of four plasmoids from a common reconnection episode. However, in this picture, the plasmoids may have all been of similar size. A slow flapping of Saturn's tail current sheet over the spacecraft (which was at constant latitude) could result in Cassini slowly moving north/south relative to the current sheet. Flapping of Saturn's current sheet is a well-documented phenomenon [e.g., Arridge *et al.*, 2011; Provan *et al.*, 2012; Volwerk *et al.*, 2013]. The flapping time scale is on the order of ~ 10 h, and thus, the 3 h shown in this plot could represent just the southward motion portion of the flapping. This idea is supported by the radial field component, which displays an increasing magnitude throughout the interval, indicating that Cassini could have been moving farther away from the current sheet center. For this case of a slowly moving current sheet, Cassini could hence have crossed near the middle of the first plasmoid and the edge of the second. As the spacecraft moved farther relative to the current sheet, it then observed a TCR and finally a weak TCR from its position in the southern lobe. The positions of the spacecraft in the plasma sheet/lobes are confirmed by inspection of the plasma data below.

Figure 5c shows the measurements from the CAPS instruments for the same interval as Figure 5a. The second and third panels are the energy-time spectrograms for the ions (above) and electrons (below) observed by the CAPS IMS and ELS, respectively. The data for the first plasmoid confirm that Cassini was inside the first plasmoid structure from $\sim 07:20$ to $\sim 07:40$, longer than the ~ 5 min duration inferred from the southward/northward field extrema above. This inference is based on the duration of the diamagnetic field signature and the presence of relatively cool dense plasma (including ions with a clear water group signature). The double-peaked ion distribution is a characteristic of plasma of inner magnetospheric origin (H^+ at low energy, W^+ at higher energy). We note that the field remains northward for some time after this interval, during the postplasmoid plasma sheet interval (as discussed by Jackman *et al.* [2011]). The three panels above the spectrograms are all-sky images of the ion distribution at 2.4 keV (first two) and 4.1 keV (third). During the first plasmoid event, the peak counts are observed near the corotation direction (black triangle) but displaced toward the look direction to Saturn, indicating an outward flow component. The energy of the ions suggests that the total flow speed is ~ 170 km/s. Based on the angular offset of the peak from the corotation triangle in the all-sky images, we suggest that the radial component of the flow is on the order of ~ 90 km s^{-1} . The plasma data for the second plasmoid support the suggestion that Cassini traversed the edge of this structure (due to the presence of hot magnetospheric electrons near 100 eV) and that the two identified TCRs were in fact observed, while the spacecraft was in the lobe (due to the absence of magnetospheric electrons and the higher spacecraft potential).

3.2. Superposed Epoch Analysis of Tailward Propagating Plasmoids and TCRs

Figures 6a and 6b depict the results of superposed epoch analyses for 69 tailward moving plasmoids and 15 tailward moving TCRs (separately), where the zero epoch is the central event time, defined as the point where B_θ changes sign. Jackman *et al.* [2011] showed a superposed epoch analysis of 34 tailward moving plasmoids, where they discussed the results in terms of the flux transport through the postplasmoid plasma sheet. Since then, as discussed in section 2, we have resurveyed the Cassini magnetometer data from 2006 and uncovered more plasmoid examples, more than doubling the list from 34 to 69. Thus, Figure 6a is an updated superposed epoch analysis. The basic characteristics of the signature are the same, with slightly amended amplitude and duration. From Figure 6a, we see that the field signature of an average tailward moving kronian plasmoid is a distinct northward turning of the field. Some individual examples display a southward turning prior to the strong northward turning, but once averaged into the superposed epoch analysis, it becomes somewhat smeared out. However, the northward turning persists. The mean plasmoid duration taken from the full set of examples listed in Table 1 is 17.71 min (with a standard deviation also of 17.7 min, implying a skewed distribution with a long tail), which represents the average duration between the local southward and northward extrema. In the absence of continuous plasma data (such as that in Figure 5c which could shed light on longer intervals of plasma energization and local tail disturbance), we interpret the interval between the southward and northward extrema as the passage of the plasmoid itself. For the case of the smeared B_θ signature from the superposed epoch analysis, we have marked the "start" of the event at

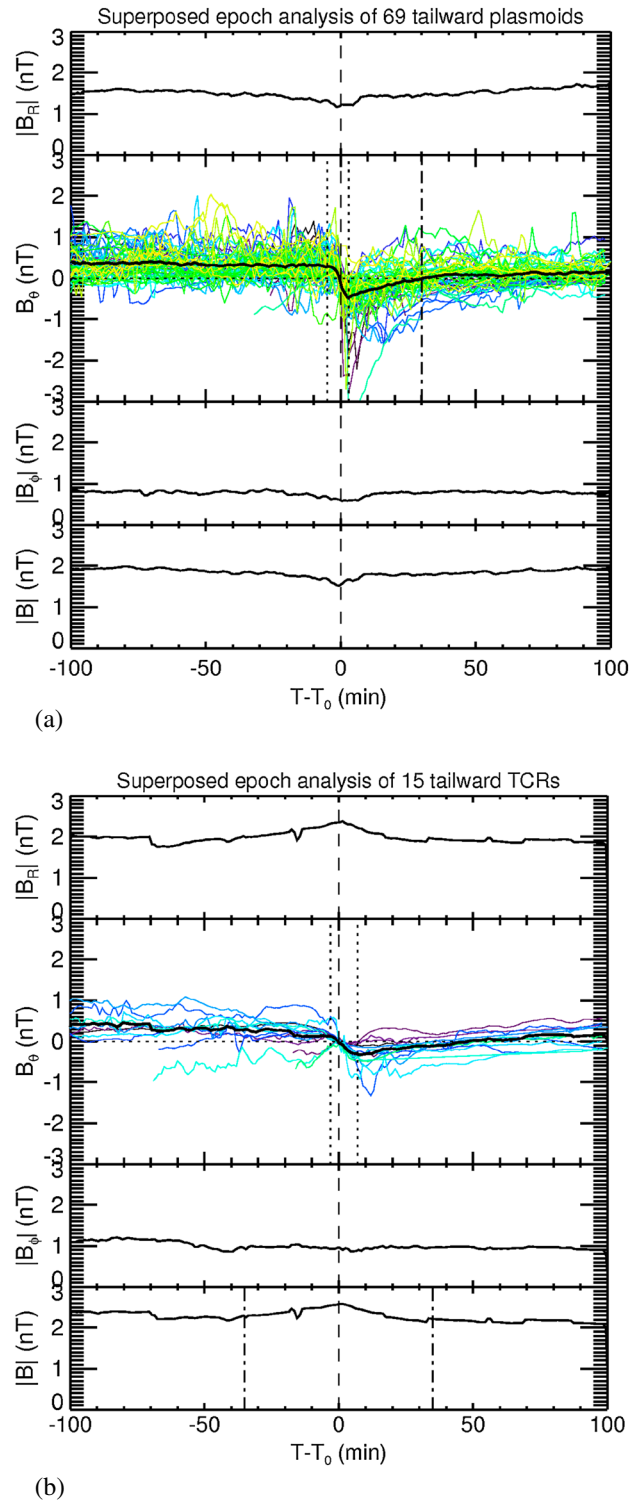


Figure 6. Superposed epoch analyses of (a) plasmoids. The second panel is twice the size and range of the other panels, and the colored lines in the second panel show the individual traces for 69 events to illustrate the spread. The thick black line shows the average trace from the superposed epoch analysis. The vertical dotted lines at $T = -5$ min and $T = +3$ min bracket the central plasmoid passage time as determined from the superposed epoch analysis. The vertical dot-dashed line marks the end of the PPPS (27 min long). (b) TCRs in the same format as Figure 6a.

$T = -5$ min despite the lack of a clear southward extremum in the trace. We obtain this start time by tracking the field fluctuations preceding the event. The B_θ component decreases slightly at $T = -6$ min, before increasing to reach a local southward maximum at $T = -5$ min, beyond which it steadily decreases and then turns northward. We note however that this local southward maximum is barely discernible above the statistical field fluctuations. This time can be compared to the mean start time (as determined from the local southward field extremum) based on 69 individual events, which is $T = -9.2$ min. The “end” of the event is marked as $T = +3$ min (the clear northward extremum). This 8 min duration is considerably shorter than the 17.71 min mean duration obtained from the distribution of events and is the effect of the smearing due to the superposed epoch analysis. Similarly, the mean ΔB_θ event amplitude from the event list is 1.39 nT (with a standard deviation of 0.73 nT), while the amplitude of the field change from $T = -5$ to $T = +3$ min is ~ 0.75 nT. Following the northward extremum (at $T = +3$ min), there is an interval ~ 27 min long, where the B_θ component remains northward. We interpret this as representing an interval of closure of previously open flux, analogous to the terrestrial PPPS. We note that there is another possibility that such asymmetry may be due to slowing of the flow as the plasmoid moves downtail, such as in cases where plasmoids associated with the Vasyliunas cycle are blocked from moving downtail by surrounding closed field lines. However, we are not in a position to test this alternative explanation of the extended northward field, because the plasma measurements available for the subset of our events simply yield a single-bulk flow speed for each event rather than a detailed time series of velocity variations throughout the interval of field change. Exploration of this hypothesis for a small number of case studies, particularly those on the dusk side where Vasyliunas-style reconnection may be more likely, should be the subject of

future work. For the purposes of this paper, we take the extended interval of northward field following the plasmoid to be representative of the PPPS and flux closure, a scenario which is consistent with auroral observations of flux opening and closing in Saturn's magnetosphere [Badman *et al.*, 2005, 2013] and modeling of reconnection and flux closure [e.g., Jia *et al.*, 2012], and we note that by making this assumption, we are taking an upper bound on flux closure for our events. While the average background B_θ at Saturn has been shown to be small and positive by Jackman and Arridge [2011], we define the end of the PPPS as the point where B_θ crosses zero to return from negative to positive for consistency. This point is marked on Figure 6a by a vertical dot-dashed line. We note that this 27 min is shorter than the ~ 58 min PPPS reported by Jackman *et al.* [2011]. The primary reason for this is that several of the new events added to the list display bipolar signatures which are more symmetric, without the extended PPPS interval of northward field after plasmoid passage. We discuss the implications of these signatures in terms of reconnection on open/closed magnetic field lines further in section 5.2.

The fact that the average southward-to-northward turning associated with plasmoid passage is strongly asymmetric hints at the geometry of the typical pass through a plasmoid, as raised initially in section 2. Due to the hinged nature of the current sheet during southern hemisphere summer, a spacecraft orbiting in the equatorial plane (as Cassini did for much of 2006) will be situated in the southern lobe, and any encounters with plasmoids will be cuts through the lower portion rather than traversals of the central part of the structures. However, we note, as illustrated in Figure 2, that a spacecraft traveling parallel to the plasmoid edge can still record a symmetric signature, even if it does not penetrate through to the center. The asymmetry arises from the spacecraft encountering the plasmoid at an angle. At the time of the field deflection shown here, there is a small local dip in $|B|$, implying a simple loop like as opposed to flux rope-like interior structure. However, this is highly sensitive to the spacecraft trajectory through the structures, and a more detailed exploration of the interior morphology of plasmoids will be presented in section 4.

The average absolute value of the radial field component during plasmoid encounters is ~ 1.2 nT, with an average of ~ 1.5 nT either side. This shows that the spacecraft did not, on average, encounter plasmoids at the very center of the current sheet (where $B_R \approx 0$) but rather at some distance away in the outer plasma sheet or lobe, as we understand from the description of the trajectory above. While the magnitude of the radial component (as a function of total field strength) cannot be used as a direct measure for vertical distance from the current sheet center, it can act as a proxy. For example, if a Harris sheet-type geometry is assumed for the plasma sheet, then fitting of the observed magnetic field to such an assumed structure can yield an estimate of distance from the center of the plasma sheet [e.g., Runov *et al.*, 2006; Arridge *et al.*, 2008; Jackman and Arridge, 2011]. Because the magnetic field data indicate the penetration of the spacecraft into a plasmoid structure, we know that in these examples, a spacecraft sampling a radial field component of magnitude ~ 1.2 – 1.5 nT cannot be more than one plasmoid half width from the center of the current sheet. As mentioned in section 2, events are identified by taking into account not just the B_θ component but the behavior of other components as well. Cassini can pass through the interior of plasmoids from a position in the outer plasma sheet but also from a position in the lobes, if the plasmoids are large enough to extend a significant distance from their formation point at the current sheet center. The azimuthal component of the field is virtually constant around the time of plasmoid passage, consistent with a loop-like picture as opposed to a flux rope-type structure as mentioned above, but this will be explored in more detail in section 4.

We can use the range of observed plasmoid durations, along with the range of observed plasmoid velocities to calculate a range of approximate plasmoid lengths (as done by Kronberg *et al.* [2008] for Jupiter and S93 for Earth). The first estimate of the velocity of a plasmoid in Saturn's tail from in situ CAPS data was presented by Hill *et al.* [2008], who reported a value of 800 km/s. Here we significantly expanded the list of events for which we can extract velocity information. From Table 1, we present a set of velocities for 29 plasmoids, ranging from 144 to 1240 km/s, with a mean of 299.8 km/s and a standard deviation of 215.5 km/s. These estimates are obtained from the energy of the peak counts and thus represent upper limits. The case study example in Figure 5c (with a total bulk velocity of 170 km/s) is at the lower end of this velocity range. We can combine this range of velocities for 29 events with the range of plasmoid durations listed in Table 1 (2 min to 50 min for the subset of 29 events for which plasma data were available). The length of each of these 29 plasmoids has been calculated individually (duration \times velocity) and is found to range from 0.44 to 23.9 R_S . The mean plasmoid length is 4.28 R_S with a standard deviation of 5.6 R_S . Figure 7 shows the histograms of flow velocity, duration, length, and mass for these 29 plasmoids which have both magnetometer and plasma data.

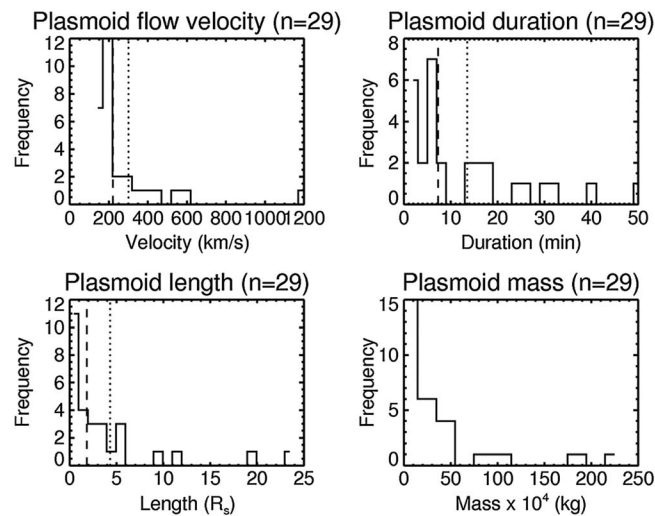


Figure 7. Histograms of plasmoid (a) flow velocity, (b) duration, (c) length, and (d) mass for the 29 plasmoid for which the magnetometer and plasma data were available. These represent a subset of the total of 69 plasmoids listed in Table 1. The vertical dotted lines are the mean values, and the vertical dashed lines are the medians.

There may be a number of errors in the determination of these plasmoid lengths. First, we note, as mentioned above, that our definition of plasmoid duration as the time between southward and northward extrema may result in an underestimate of plasmoid size by a factor of ~4–8 [Kivelson and Khurana, 1995]. In addition, the duration estimates are based on trajectories which, as discussed earlier, do not necessarily represent the full diameter of the plasmoids. Unless the observing spacecraft passes through the center of the plasmoid along a trajectory that is normal to the long axis of the structure, the effective length of the plasmoid may be significantly underestimated or overestimated. There are also errors associated with the velocity measurements. The velocities used to

determine the plasmoid “lengths” are the bulk flow velocities, and from the subset of examples where CAPS pointing was favorable, we know that in addition to the radial (downtail) component of the velocity there can also be a significant azimuthal motion. Hence, the bulk flow velocity is an upper limit. We may compare our estimates of plasmoid length derived here with the output of global models, which suggest that plasmoids may be up to 30–40 R_S long [e.g., Jia et al., 2012; Kidder et al., 2012]. Such estimates are higher than our quoted range, but we note that the model estimates consider the full plasmoid and not just a cut through a section, as may be the case for our examples.

In addition to our estimates of plasmoid length, we can use the velocity measurements to estimate the size of the reconnecting region and in turn estimate the flux closed through reconnection. As mentioned above, the superposed epoch analysis shows a distinct ~27 min after plasmoid passage where the field remains northward, analogous to the terrestrial PPPS. Jackman et al. [2011] calculated the amount of flux closed during a ~58 min PPPS as obtained from the superposed epoch analysis of 34 events. They assumed a velocity of 800 km/s [Hill et al., 2008] and took an upper limit of the full tail width (90 R_S) for the azimuthal extent. From this, they calculated a flux closure of ~3 GWb per event.

We now have an extended sample of events which yield an ~27 min PPPS, the length of which is also subject the same kind of assumptions made above regarding the orientation of the plasmoid motion relative to the spacecraft. We also have additional in situ data which allow us to make flux estimates based on a range of velocities. Like Jackman et al. [2011], we use the full tail width of ~90 R_S as the azimuthal extent of the plasmoid for our calculation, emphasizing that this 90 R_S value is an upper limit. In reality, we expect that the typical width of reconnection-associated flow channels in the tail is much smaller than this, because if plasmoids took up the full width of the tail, Cassini would observe every one as long as its position was tailward of the reconnection site. Based on the speeds of 144–1240 km/s, we estimate that 0.26–2.2 GWb of flux is closed during the 27 min PPPS.

The TCR superposed epoch analysis for 15 tailward moving events, shown in Figure 6b, shows the localized compression associated with the wrapping of field lines around the passing plasmoid(s). This smooth increase in the total field strength is also mirrored by a smooth increase in the radial field component, peaking at the center of the TCR. The average amplitude of the southward-to-northward turning from the list of 15 events is ~0.66 nT (with a standard deviation of 0.54, reflecting the wide spread in amplitude of TCR signatures). This amplitude is slightly smaller than for the plasmoid encounters as might be expected (particularly considering that our selection criteria did not require the B_θ component during TCRs to fluctuate above background levels). The average TCR signature at Saturn displays a mean change in $|B|$ of ~18%. This is

compared to typical compression ratios of 1–10% at Earth [Slavin *et al.*, 1993; Slavin *et al.*, 2005]. Thus, this is an evidence that plasmoids at Saturn are large enough to significantly distort the magnetotail field lines in their vicinity and could imply that plasmoids at Saturn occupy a larger vertical portion of the magnetotail than plasmoids at Earth, although this cannot be confirmed with a single spacecraft. In some cases at Earth, it is suggested that waves initiated at the center of the plasma sheet during reconnection can travel through the lobes all the way to the magnetopause, communicating field disturbances such that the magnetopause may even exhibit a corresponding bulge; however, this behavior is still not fully understood [Slavin *et al.*, 1993]. The average duration of the 15 observed TCRs, as defined by the time between local maxima/minima in B_θ either side of the central field deflection, and as calculated from the list in Table 1, is 14.4 min (with a standard deviation of 9.35 min). As with the plasmoid superposed epoch analysis, the TCR superposed epoch trace becomes somewhat smeared out, and thus, its amplitude and duration (~ 0.43 nT from $T = -3$ to $T = +7$ min) are considerably smaller than those calculated directly from the distribution. However, on the inspection of the field magnitude trace, it is clear that $|B|$ undergoes a smooth compression from background levels over a much longer interval, on the order of ~ 35 min either side of the central epoch time, 70 min in total, as bracketed by the vertical dot-dashed lines in the fourth panel.

4. Morphology of Reconnection Region

While reconnection undoubtedly has dramatic effects on the local structure of the field lines in the vicinity, it can also affect the global morphology of the magnetotail. As discussed in section 3.2, the passage of large plasmoids downtail can cause the surrounding lobe field lines to bend significantly as they wrap around the bulging plasma sheet. In the Introduction, we mentioned that plasmoids may have loop-like or flux rope-like interior structure, and these structures have implications for the structure of the magnetotail as a whole, perhaps elucidating the degree of shear within the tail prior to reconnection. In this section we examine the Cassini magnetic field data in detail to decipher the nature of the field geometry in Saturn's tail when reconnection is ongoing.

In order to precisely visualize the geometry of the reconnection region, we apply minimum variance analysis (MVA) to several events [Sonnerup and Cahill, 1967]. Transforming the magnetic field data into this coordinate system allows us to visualize the orientation of the structures and the location of their central axis. When MVA is performed on a magnetic field data set, it returns three eigenvectors (corresponding to the minimum, intermediate, and maximum variance directions) and their associated eigenvalues. The direction which corresponds to the axis of the structure depends on the type of structure and on the depth of crossing (known as the impact parameter). For a crossing close to the center of a cylindrically symmetric force-free flux rope, the intermediate direction is the direction of the axis [e.g., Lundquist, 1950; Lepping *et al.*, 1990]. The perfectly force-free flux rope is a special case, representing the minimum energy state of a structure. At the center, the field is purely axial, and this field weakens with increasing distance from the center. In practice, many magnetotail plasmoids take the form of non-force-free flux ropes, which also have a helical topology but have not yet evolved to a force-free configuration. In this case the structure has a core field (such as those studied at Venus by Russell [1990] and Elphic and Russell [1983]), and the axis may be oriented with the intermediate or maximum directions. A third class of structure is loop-like plasmoids. In reality, it might be difficult to expect perfect loops to form in three-dimensional space as this requires perfect alignment of oppositely directed magnetic field lines [e.g., Slavin *et al.*, 2003a]. However, quasi-loop-like structures should be distinctive in terms of having their axes aligned along the minimum variance direction [Farrugia *et al.*, 1987; Elphic and Southwood, 1987]. Clearly, the determination of the orientation of the axis of plasmoids is key to the study of their geometry, structure, and their possible formation process.

The interval over which the MVA is performed is crucial to the success of the analysis. A first criterion for a good MVA interval is that it encompasses the largest field change associated with the passage of the plasmoid, TCR, or dipolarization. Second, a large eigenvalue ratio gives confidence in the transformation. Previous studies have indicated that the ratio of intermediate to minimum eigenvalue should be at least ~ 8 – 10 for the analysis to be acceptable [e.g., Paschmann and Daly, 1998; Briggs *et al.*, 2011]. The largest eigenvalue ratios tend to result from the selection of intervals which bracket the turning points of bipolar magnetic field signatures, thus encompassing the greatest change of magnetic field strength and direction.

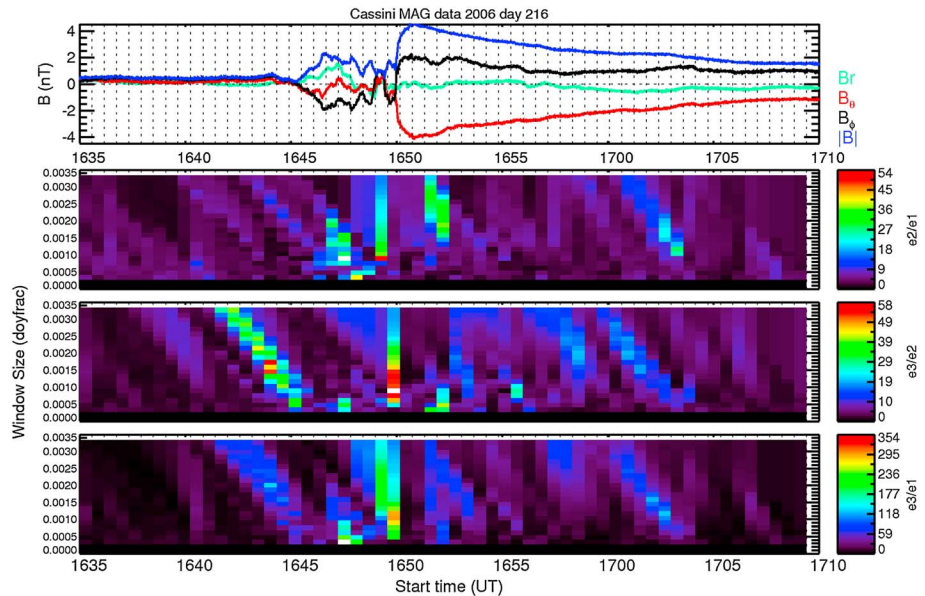


Figure 8. Example of MVA optimization technique applied to magnetometer data from 2006 day 216 16:35–17:10. The first panel shows the magnetic field data in KRTP coordinates, color coded according to the legend on the top right. The next three panels show the results of the application of a sliding window for MVA. On the x axis are the various start times of the MVA windows (also denoted by the vertical dashed lines in the first panel). The y axis shows the window sizes, applied from each start point. Thus, the plots are composed of a selection of boxes which represent various start times and window lengths over which MVA was applied. The colors (coded as per the color bars on the right-hand side of the plots), show the eigenvalue ratios, for e_2/e_1 , e_3/e_2 , and e_3/e_1 , respectively. B1 is the direction of minimum variance, and B2 and B3 refer to the intermediate and maximum variance directions.

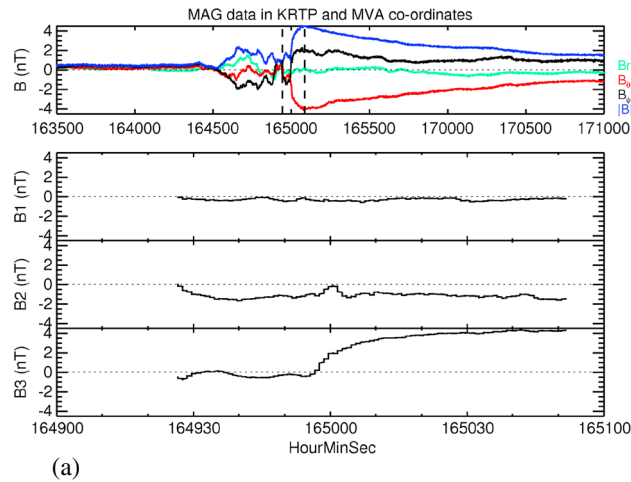
4.1. MVA Window Optimization Technique

Throughout this work, we have sought to remove observer biases as much as possible. For example, the selection of an appropriate MVA window is most often done “by eye,” and while this may be satisfactory for most cases, we desired to try an automated method to select the interval over which the field changes most significantly and to then apply the MVA to this interval. This “MVA window optimization” technique is illustrated in Figure 8.

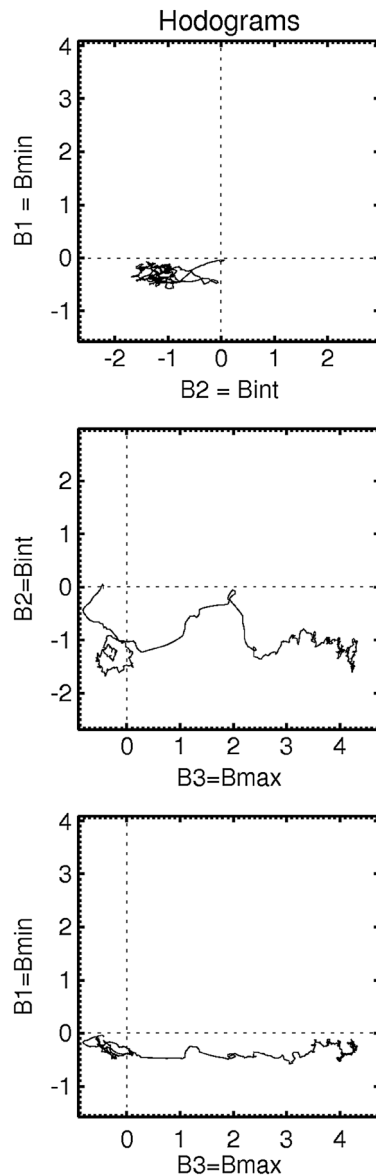
The first panel shows the field in KRTP coordinates, color coded according to the legend on the right. The feature of interest is a plasmoid at 16:47:30, identified by the strong northward turning of the field (negative B_θ in red). MVA was applied to this field data over a sliding window, with start times marked by the vertical dotted lines. The start times and window sizes are plotted on the axes of the lower three panels, which are color coded to show the eigenvalue ratios for each MVA start time and window size. The darker colors represent the lower eigenvalue ratios, as per the color bars on the right of each of the lower three panels. The striking feature of this plot is that the eigenvalue ratios corresponding to start times and window sizes away from the main plasmoid observation are low. Meanwhile, the eigenvalue ratios increase significantly in the vicinity of the northward turning. Indeed, there is a bank of high eigenvalue ratio intervals surrounding the main northward turning. This gives us confidence that selecting an MVA interval in this region will return sufficiently high eigenvalue ratios such that we can be satisfied that the analysis interval encompasses the most significant field change. While the maximum eigenvalue ratio is not a perfect marker of where the MVA

Table 2. List of Eigenvectors and Eigenvalue Ratios for All the MVA Intervals Described in Section 4.2

Eigenvectors	B1 (Minimum)	B2 (Intermediate)	B3 (Maximum)	L2/L1	L3/L2
Day 216 plasmoid, 16:47:30	(0.99, 0.08, 0.02)	(0.07, -0.70, -0.71)	(0.05, -0.71, 0.70)	6.53	42.9
Day 63 plasmoid, 22:07	(-0.89, -0.15, -0.44)	(0.35, 0.39, -0.85)	(-0.30, 0.91, 0.29)	9.26	15.6
Day 63 plasmoid, 22:59:30	(0.77, -0.27, -0.58)	(-0.61, -0.05, -0.80)	(-0.18, -0.96, 0.19)	44.7	37.0



(a)



(b)

should be applied, it acts as strong guide. We note that the three eigenvalue ratios rarely maximize in precisely the same windows. Nonetheless, the plot indicates that the eigenvalues maximize in broad regions surrounding the field change of interest. This technique then gives us confidence to apply MVA over the window bracketing the south-north extrema in B_θ either side of the primary field deflection. We also recognize that changing the MVA window size may alter the orientation of the axis that we obtain from our analysis. Thus, MVA has been tested over several window sizes within this central high eigenvalue ratio region to ensure the stability of the orientation.

4.2. MVA Examples

For all the three subsequent examples, we use the optimization technique outlined above to guide our choice of MVA analysis window. The eigenvectors and eigenvalue ratios are listed in Table 2.

4.2.1. MVA Example 1: Day 216 (4 August) Plasmoid, 16:47:30

Figures 9a and 9b show the results of the application of MVA over a window surrounding the plasmoid on day 216 at 16:47:30. Vertical dashed lines on the first panel of Figure 9a bracket the interval on which the MVA was performed. The lower three panels show the magnetic field data transformed into MVA coordinates and plotted over the selected interval (less than 2 min long). B1 is the direction of minimum variance, and B2 and B3 refer to the intermediate and maximum variance directions. The spacecraft was $49 R_S$ downtail and just premidnight at 23:41 LT. This event was reported first by *Jackman et al.* [2007], while *Jackman et al.* [2008a] showed that the large-scale magnetospheric plasma flow rotated

Figure 9. (a) Results of minimum variance analysis on an interval of magnetic field data from 2006 day 216. The first panel shows the magnetic field in KRTP coordinates. The vertical dashed lines denote the interval over which MVA was applied. The selection of this interval was guided by the optimization technique outlined in Figure 9. The lower three panels show the field minimum, intermediate, and maximum variance directions (b). Field hodograms for the interval selected in Figure 9a.

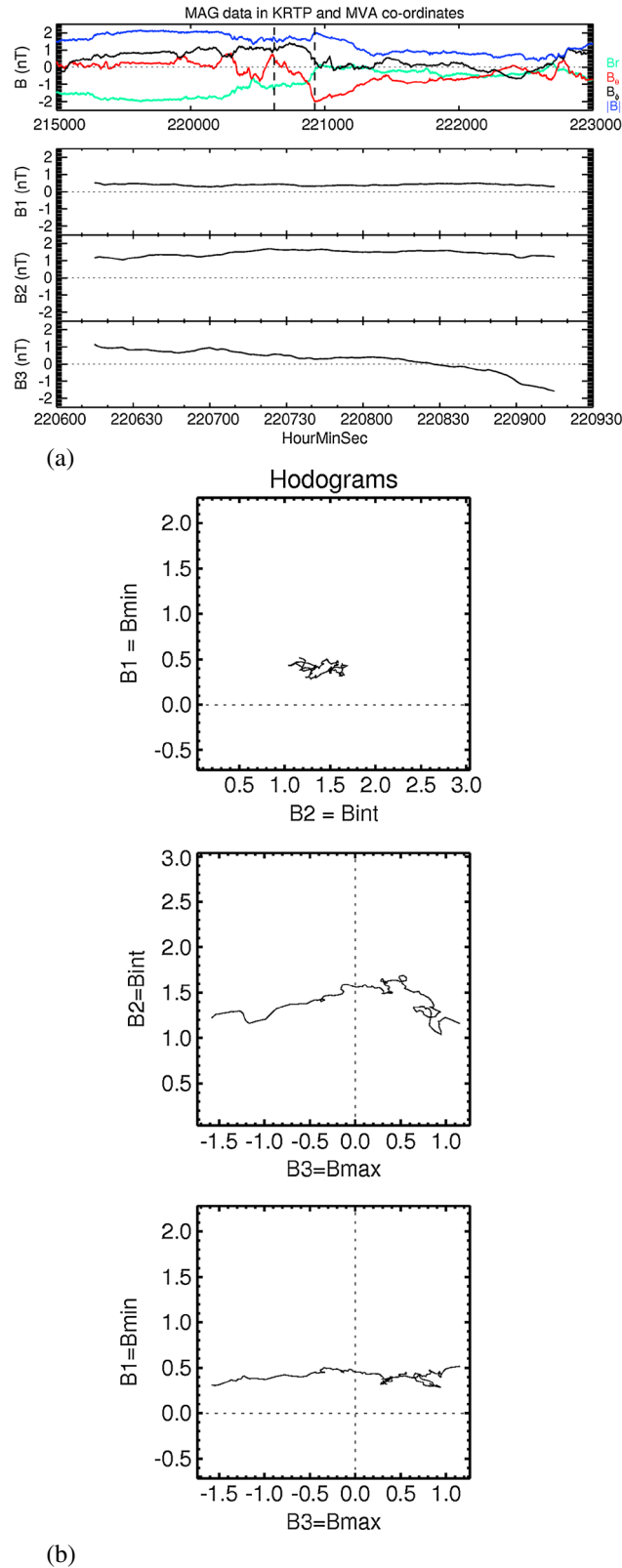


Figure 10. (a) Magnetic field in KRTP and MVA coordinates surrounding a plasmoid observation on 2006 day 63 at 22:07. The figure is in the same format as Figure 9a. (b) Field hodograms corresponding to the interval depicted in Figure 10a.

from subcorotation to tailward with the passage of this plasmoid. The plasma data from CAPS IMS (not shown) indicate the presence of outward moving W^+ ions during the passage of this plasmoid. The field signature is certainly dramatic, with a total field deflection of 3.39 nT. The total field strength rises sharply coincident with plasmoid passage, and this has been interpreted as pile up of newly closed field lines behind the plasmoid after reconnection, accelerating its downtail. The field in the direction of minimum variance (B1) is near zero, while the intermediate variance trace (B2) is unipolar. The dominant northward turning of the field associated with plasmoid passage is reflected in the maximum variance direction, which displays a dramatic bipolar signature. The eigenvectors are (0.996, 0.084, 0.018), (0.072, -0.697, -0.714), and (0.047, -0.712, 0.700), indicating that the direction of minimum variance is strongly radial, the intermediate variance direction is split between northward and corotational, and the maximum variance direction is split between northward and corotational. Figure 9b shows the hodograms of the field variations in three planes, with most variation in the intermediate-maximum plane. The near-constant, nonzero minimum, and intermediate fields combined with the predominantly positive maximum variance argue for Cassini having just passed through the outer portion of this plasmoid along a trajectory that began in the south, but quickly passed into the northern half of the plasmoid (e.g., see trajectory path #4 in Figure 2). No flux rope-line core field was observed, but it cannot be determined whether this is due to the plasmoid being loop-like or the off axis trajectory.

4.2.2. MVA Example 2: Day 63 (4 March) Plasmoid, 22:07

Figure 10 shows the results of MVA on an interval surrounding a tailward moving plasmoid at 22:07 on day 63 of 2006. At this time, the spacecraft was $44.17 R_S$ downtail and at a local time of 03:10. The plasmoid is identified by the deflection in the B_θ component northward, with an

amplitude of 1.7 nT. The more balanced north-south magnetic field variation shows that the spacecraft passed much closer to the center of this plasmoid than the previous event. Once again, B1 is approximately constant near zero and directed largely in the radial direction consistent with a pass not far off the center of the plasmoid. B2 is mostly azimuthal and unipolar, but it does not display any enhancement near the inflection point in the north-south field as would be expected if there were a flux rope-type core field. B3 is closely aligned with the north-south direction and shows a bipolar signature. The eigenvectors are $(-0.887, -0.151, -0.436)$, $(0.350, 0.395, -0.849)$, and $(-0.300, 0.906, 0.298)$, indicating that the direction of minimum variance is primarily radial, the intermediate variance direction is in the corotation direction, and the maximum variance direction is north-south. We suggest that this example could represent a passage through a loop-like plasmoid, along a trajectory similar to path #2 in Figure 2, although closer to the center of the structure than the encounter in MVA example 1 on day 216. Figure 10b shows the hodograms of the field variations in three planes. The B2-B3 hodogram shows a relatively smooth tilting of the field consistent with a loop-like plasmoid. This can be compared to an example of a rare but well-defined magnetic loop plasmoid at Earth reported by *Slavin et al.* [1989].

4.2.3. MVA Example 3: Day 63 (4 March) Plasmoid, 22:59:30

Figure 11a shows high-resolution Cassini magnetometer data surrounding a plasmoid observation at 22:59:30 on day 63 of 2006. At this time, the spacecraft was $44.17 R_S$ downtail and at a local time of 03:11, virtually the same location as for the previous example less than an hour before, although in this example, the magnitude of the B_R component is somewhat smaller indicating that the spacecraft was situated closer to the current sheet center. The plasmoid is identified by the sharp northward turning of the field of amplitude 3.51 nT, and the balance between northward and southward magnetic field. It is followed by an extended interval of northward field, which we interpret as analogous to a postplasmoid plasma sheet as at Earth. The field change associated with the plasmoid passage is very rapid, and the MVA is performed over an interval of <50 s long, using the highest-resolution magnetometer data available. The eigenvectors are $(0.772, -0.264, -0.578)$, $(-0.608, -0.045, -0.792)$, and $(-0.183, -0.963, 0.195)$. The field in MVA coordinates shows the clear signature of a plasmoid with flux rope topology. The constant, near-zero B1 (min) directed along the radial direction is consistent with a very low inclination spacecraft trajectory passing through the center of the plasmoid similar to the green traces (trajectory path #1) in Figure 2. The B2 (intermediate) component is unipolar, peaked around the center of the bipolar north-south field variation, and oriented in the azimuthal direction consistent with a cross-tail oriented flux rope (Figure 2, bottom) [e.g., *Slavin et al.*, 2003a; *Borg et al.*, 2012] with the core in the B2 (intermediate) direction. The B3 (maximum) direction is largely in the north-south theta direction and displays the expected clear bipolar trace. The B2-B3 hodogram shows exceptionally smooth rotation indicative of the core magnetic field of a flux rope-type plasmoid.

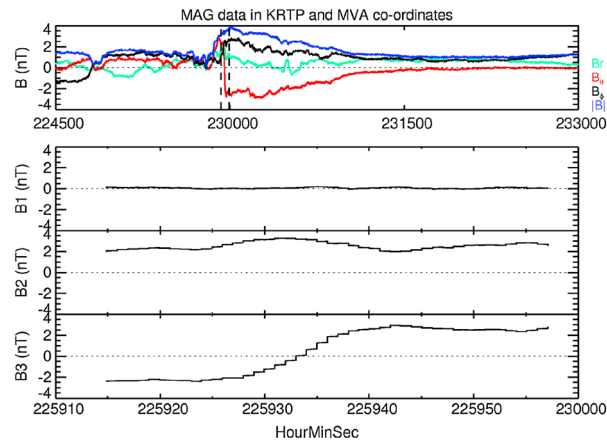
5. Discussion

In this paper we have presented a set of reconnection events observed during Cassini's exploration of Saturn's deep tail during 2006. We now discuss the results by placing them in the framework of several common questions about the nature of reconnection in Saturn's tail.

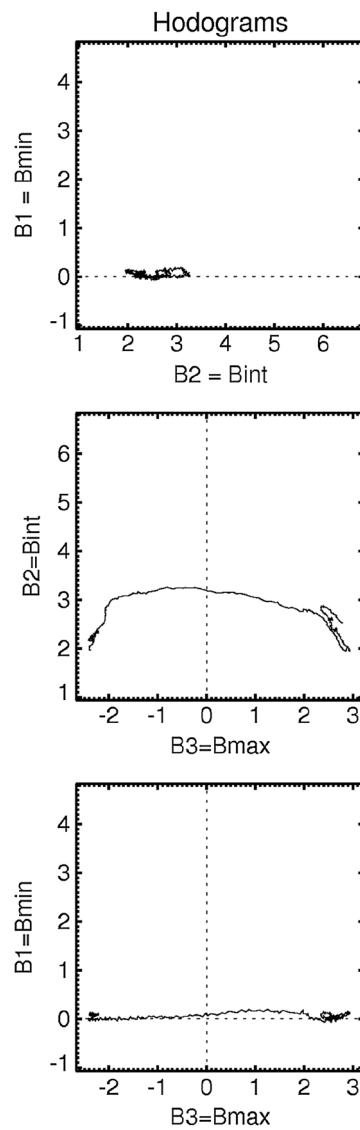
5.1. What is the Primary Mass Loss Mechanism at Saturn?

In this study we have revealed 69 south-to-north plasmoids tailward of the x line, 17 TCRs (15 tailward and 2 planetward), and 13 north-to-south events planetward of the x line, which represent the largest and most significant reconnection signatures from our detailed survey of the 2006 Cassini magnetometer data. The question remains however as to whether there are mechanisms other than large-scale reconnection, which may allow material to be lost down the magnetotail. For instance, *Zieger et al.* [2010] suggested on the basis of their modeling work that large-scale plasmoids account for less than 8% of the total mass lost down the tail. *Bagenal and Delamere* [2011] estimated the average mass of plasmoids at Saturn and compared this to the suggested mass loading rates from the moon Enceladus of 8–250 kg/s [e.g., *Fleshman et al.*, 2010; *Jurac and Richardson*, 2005; *Pontius and Hill*, 2009; *Chen et al.*, 2010]. They assumed a plasmoid of volume $(10 R_S)^3$ with a density of 0.01 cm^{-3} of 18 amu ions. From this, they calculate that plasmoids would need to be ejected at a rate of 200/d to remove just 100 kg s^{-1} .

We are now in a position to refine the estimates of the plasmoid mass loss rate. We base our calculations on the 29/69 plasmoids which have corresponding plasma data. We calculated the length for each plasmoid as



(a)



(b)

Figure 11. (a) Magnetic field in KRTP and MVA coordinates surrounding a plasmoid observation on 2006 day 63 22:59. The figure is in the same format as Figure 9a. (b) Field hodograms corresponding to the interval depicted in Figure 11a.

duration \times velocity and obtained a range of $0.44\text{--}23.9 R_S$. We note that these observed speeds sit between the estimates of average Alfvén speeds in Saturn’s central plasma sheet ($1\text{--}10$ km/s) and lobes (>4000 km/s) as reported by *Arridge et al.* [2009]. They also agree reasonably well with analogy from Earth, where plasmoids have been observed to move tailward with speeds typically 1–3 times that of the solar wind [*Baker et al.*, 1987; *Richardson et al.*, 1987; *Ieda et al.*, 1998; *Slavin et al.*, 2003a]. If we average all of the plasmoid lengths obtained in this way, we find a mean of $4.28 R_S$ (whereas if we multiply the mean duration of 13.5 min by the mean velocity of 299.8 km/s, we obtain a mean plasmoid length of $4.03 R_S$). We take a thickness of $2 R_S$ to represent the plasma sheet half-thickness (for a full plasma sheet width of $4 R_S$ [e.g., *Kellett et al.*, 2009; *Sergis et al.*, 2011; *Arridge et al.*, 2011; *Szego et al.*, 2012]), and we take an upper limit for the azimuthal extent as the full tail width ($90 R_S$). Because this estimate is intended to represent an upper limit, instead of assuming the same density as *Bagenal and Delamere* [2011] (0.01 cm^{-3} of 18 amu ions), we take the upper limit from *Thomsen et al.* [2014] of 0.1 cm^{-3} of 16 amu ions. We thus calculate a range of plasmoid masses from $4.42 \times 10^4\text{--}241.0 \times 10^4$ kg, with a mean of 43.2×10^4 kg. We would require $\sim 3.6\text{--}196$ tail-width plasmoids per day to remove 100 kg s^{-1} of added mass. In order to estimate the total mass loss for the 99 reconnection events that we observe, we multiply the mean plasmoid mass of 43.2×10^4 kg by 99 events. Our events were observed between days 32 and 264 of 2006. If we calculate how much time the spacecraft spent beyond $20 R_S$ on the nightside during this interval (to give an approximate likely “viewing region” for downtail mass loss) and express

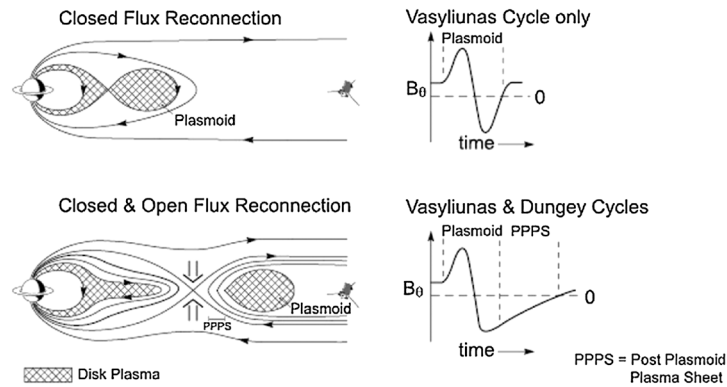
the total mass loss as a fraction of time, we find an average mass loss rate over our observation interval of 2.59 kg/s.

There are several “active” intervals during 2006, where multiple plasmoids and TCRs are clustered together, such as: days 60–67 inclusive (18 events), days 193–197 inclusive (13 events), and days 212–219 inclusive (15 events). Indeed, there are 6 events on day 212 alone (~23:00 h local time and between 43 and 45 R_S). Thus, it appears that during the most active intervals, the observed rate of mass loss can just about match the lower end of the requirement for removal of 100 kg/s of mass (and easily match the requirement for a lower mass source rate of 8 kg/s). However, there is a huge range on the mass removal requirements, and during less active intervals, there is a clear mismatch between the suggested loading rates and observed average removal rates. Thus, it is plausible that during active intervals, plasmoid ejection at Saturn is the primary mass loss mechanism. However, we need to explain the significant mismatch in mass addition and loss rates during the more typical, less active intervals. There may be several reasons for this mismatch. First, we may only be observing a small fraction of the number of plasmoids that are released in Saturn’s tail. We may be missing examples due to spacecraft trajectory out of the plane of the plasma sheet. Similarly, we may miss a large number of plasmoids released via the Vasyliunas cycle [Vasyliunas, 1983] down the dusk flank (if, as stated in section 3.2, the real azimuthal extent of plasmoids is much less than 90 R_S). We return to the issue of the difference between Vasyliunas and Dungey cycle reconnection in the next section. A second reason for the mismatch may be in the scale of the events. If a steady stream of small-scale plasmoids were to be released, the cumulative effect could go a long way toward making up the mass deficit. As outlined in section 2, the events that we identify are the clearest, largest amplitude events from the Cassini magnetometer data in 2006. There may be many smaller-scale events with field signatures close to the level of background fluctuation that we have not selected here as we did not deem them to be unambiguous. Third, there may be other mechanisms for mass loss in Saturn’s magnetosphere apart from reconnection. *Bagenal and Delamere* [2011] suggested that perhaps cross-field diffusion, “drizzle” from highly stretched dusk field lines, or other small-scale loss mechanisms may account for much of the mass loss from the tail, particularly down the dusk flank [e.g., *Kivelson and Southwood*, 2005]. A final possible reason is that the spacecraft did not sample far enough downtail to capture major plasmoid ejections from a possible distant x line. The question of how mass is lost from Saturn’s magnetosphere is certainly one which warrants further investigation. For comparison, we refer the reader to *Vogt et al.* [2014] for a discussion of the minor role of plasmoids in mass loss in the jovian magnetotail.

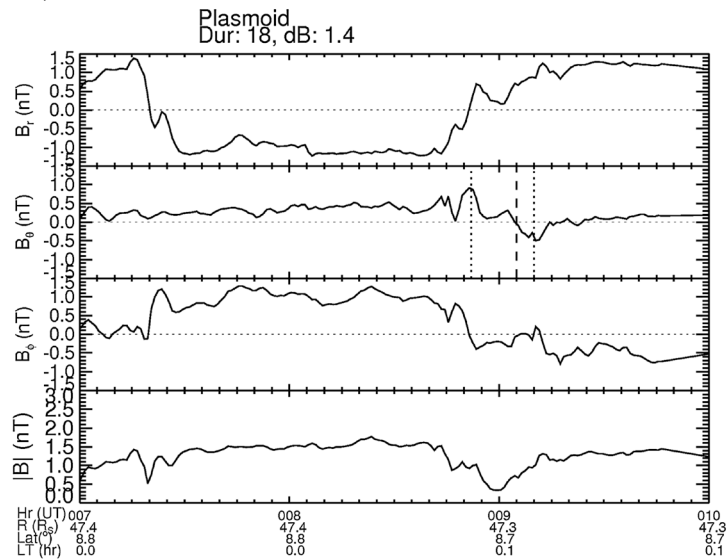
5.2. What Drives Reconnection at Saturn?

The Dungey and Vasyliunas cycles at Saturn are the primary cycles of magnetospheric convection. The Dungey cycle is driven by interaction with the solar wind and involves the opening of flux via reconnection at the dayside and the closing of it on the nightside, with return of empty flux tubes to the dayside primarily via dawn. The Vasyliunas cycle is an internally driven process, involving the rotation of mass-loaded flux tubes down the dusk flank and pinch off primarily premidnight. Reconnection and associated plasmoid loss can complete the cycle of magnetospheric convection at Saturn in both the Dungey and Vasyliunas regimes [Cowley *et al.*, 2004]. Theory predicts that both processes exist at Saturn [Badman and Cowley, 2007], and evidence for Vasyliunas cycle return flow from plasma data has been presented [Masters *et al.*, 2011]. *Jackman et al.* [2011] posed the question of whether the nature of the reconnection field signatures could help to distinguish the difference between the reconnection of closed (Vasyliunas-cycle) and open (Dungey-cycle) field lines. They interpreted the presence of a significant PPPS at Saturn as evidence of a significant closure of open flux. We note that even if reconnection is initially driven by the Vasyliunas cycle, the reconnection can proceed from closed field lines to open within a single episode, thus closing previously open flux via “Dungey-type” reconnection.

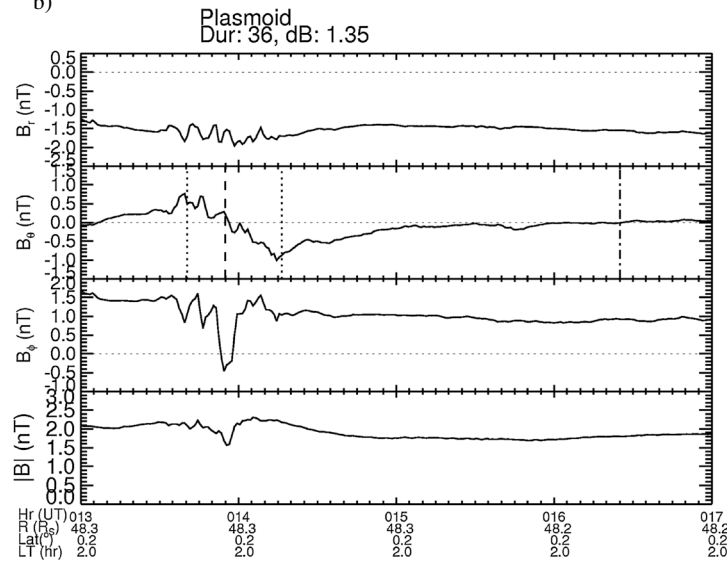
Figure 12 includes a cut from the picture presented by *Jackman et al.* [2011] and shows two contrasting examples of plasmoids from the newly updated set. The panels show the schematic pictures of textbook “bipolar” and “PPPS” signatures, while Figures 12b and 12c show real examples of such events from the magnetometer data. We did not have a large enough number of events such as these to explore any local time dependence of the features. In this work, we found the vast majority of plasmoids at Saturn displayed some extended interval of northward field following plasmoid passage. We have interpreted this as representative of an interval of closure of open flux or a PPPS. However, we note the alternative explanation



a)



b)



c)

Figure 12. (a) Schematic of the expected field signatures for reconnection on closed and open field lines. (b) Cassini magnetometer data from 2006 day 243 07:00–10:00. A plasmoid was observed at 09:05. The central event time, (where B_θ goes through zero), is marked by the vertical dashed line, while vertical dotted lines either side of this mark the start and end points of the event. (c) Cassini magnetometer data from 2006 day 131 13:00–17:00 in the same format as Figure 12b. The vertical dot-dashed line marks the end of the PPPS.

for the PPPS field signature given in section 3.2, in which plasma can be slowed due to Vasylunas-style reconnection occurring and plasmoids being trapped within outer closed field lines. The exploration of such a scenario should be the topic of future detailed case study analysis with high-resolution plasma data. For the purposes of this paper, we base our PPPS interpretation on analogy with Earth, where a PPPS is a common feature [e.g., Richardson *et al.*, 1987] to explain such a distinctive field signature. In doing so, the flux values we derive for Saturn can represent an upper limit to the rate of closure of open flux in this process (within the limit of our assumptions). We also compare with studies of Saturn's aurora which show changes in the auroral oval size linked to changing flux content of the polar cap [e.g., Badman *et al.*, 2005, 2013]. These studies suggest that opening and closing of magnetic flux via dayside and nightside reconnection are significant processes in Saturn's magnetosphere. Plasmoid release and subsequent reconnection of open lobe field lines must play a part in this picture.

Figure 12b shows an example event from 2006 day 243. The interval shown is from 07:00 to 10:00, and the plasmoid in question is observed at 09:05, when the spacecraft was $47.3 R_S$ downtail at a local time of 00.1 h. The B_R trace indicates that the current sheet moved over the spacecraft just before plasmoid passage such that Cassini moved from southern lobe to the plasma sheet north of the current sheet and into the northern lobe during the event. Plasma data (not shown) confirm this picture. The B_θ field signature displays the textbook bipolar signature, which may be associated with reconnection on closed field lines as depicted schematically in Figure 12a.

Figure 12c shows a plot of Cassini magnetometer data from 2006 day 131 13:00–17:00. A plasmoid is observed passing tailward over the spacecraft at 13:55, when the spacecraft was at a radial distance of $\sim 48.3 R_S$ downtail, at ~ 02 LT. The duration of the plasmoid itself was 36 min, during which there was a total field deflection of 1.35 nT. However, this signature was followed by a long interval, where the field remained northward. Indeed, B_θ only reached zero again at 16:25. This field signature is in sharp contrast to the bipolar signature observed in Figure 12b.

As mentioned above, plasmoid loss is expected for both the Vasylunas and Dungey cycles. In some theoretical pictures of Saturn, Dungey cycle reconnection is predisposed toward the dawn flank [e.g., Cowley *et al.*, 2004]. Work at Jupiter has suggested a pattern of reconnection in which stretching empties flux tubes on the evening side, and they snap back and then stretch out again postmidnight [Kivelson and Southwood, 2005]. We clearly require a large sample of magnetic field and plasma data in order to understand the global patterns of plasma circulation. While the single textbook "Vasylunas-style" bipolar B_θ signature case study shown here was observed premidnight, we do not have a sufficient number of "Vasylunas-type" events to say whether this is the case on average. A longer-term goal of the study of Saturn's tail should be to exploit all the available dusk coverage by Cassini (albeit at smaller radial distances than the 2006 trajectories) to understand the mass loss in this understudied region.

5.3. Where Does Reconnection Happen and What is the Size of the Affected Region?

In the well-sampled terrestrial magnetosphere, the role of magnetic reconnection in driving magnetospheric convection is well established [Baker *et al.*, 1996]. However, much remains to be understood regarding the nature and effectiveness of external triggers for the onset of reconnection [Hsu and McPherron, 2003] and the factors affecting the number of events and the location of x -line formation [e.g., Imber *et al.*, 2011]. In this paper we have reported 69 tailward moving plasmoids, 17 TCRs, and 13 planetward moving events. As mentioned in the introduction, the sign of the change in B_θ over time (north-to-south or south-to-north) indicates which side of the x line the spacecraft is on. In our case, the vast majority of the events were observed to be moving tailward. Even with an expanded database of planetward moving events, it has been impossible to derive a statistical separatrix based on field change or flow patterns in the same sense that others have employed at Jupiter [e.g., Woch *et al.*, 2002; Vogt *et al.*, 2010].

Estimates from ENA observations place the near-planet x line at radial distances of ~ 20 – $30 R_S$ [Mitchell *et al.*, 2005]. However, we note that ENA emission is stimulated when energetic particles interact with the neutral torus at Saturn, and thus, the observation of ENA emission from this radial range can simply mean that this is where excitation took place, rather than pinpointing where reconnection originated. Modelers have also sought to explore the issue of the x -line location. Jia *et al.* [2012] suggested that the x -line position at Saturn can vary from 25 to $40 R_S$ depending on solar wind dynamic pressure, with the x line moving toward the planet and

becoming narrower when the magnetosphere is compressed. Our results would seem to qualitatively agree with the conclusions of modeling work, suggesting that the position of the x line is highly variable.

The timing of reconnection onset was discussed by *Russell et al.* [2008], who postulated a relationship between reconnection onset and the position of the moon Titan in local time based on 6 events. We have tested this relationship with the much larger data set presented in this paper, and we do not find that the position of Titan is statistically significant in terms of linking to reconnection event observation.

We noted above that from the subset of plasmoid events with plasma velocity information, we can estimate the average plasmoid length at $\sim 0.44\text{--}23.9 R_S$. We note however that these numbers are highly sensitive to trajectory effects, as spacecraft passes through the plasmoids may take the form of “cords” through the edge as opposed to direct traversals of the central/widest part of the structures. Also, this calculation of “length” is based on the assumption that plasmoids travel radially downtail after ejection and neglects any azimuthal motion. The azimuthal extent of the reconnection region is not well constrained. At Earth, the flow channel widths associated with bursty bulk flows are observed to be $\sim 1\text{--}2 R_E$ [*Angelopoulos et al.*, 1996], just less than 10% of the width of the Earth’s tail. However, this applies to the planetward moving portion, which will be azimuthally limited. At Jupiter, *Vogt et al.* [2010] found that the mean flow channel width associated with reconnection in the jovian tail is $18 R_J$, 6.67–10% of the typical tail width, a value which they suggested to be a lower bound, taking measurement uncertainties into consideration. In the absence of multiple spacecraft or continuous plasma velocity measurements at Saturn, we are unable to constrain the corresponding values. However, one must remember that once released, plasmoids are free to expand to achieve pressure balance with their local surroundings, and thus, we might expect the azimuthal extent to represent a larger portion of the tail width with increasing distance downtail.

In terms of local time, Figure 4c shows that there are many more observations of reconnection events postmidnight than premidnight. The theoretical picture put forward by *Cowley et al.* [2004] suggested that reconnection on closed field lines occurs predominantly in the dusk sector, with Dungey cycle open field line reconnection dominating toward dawn. *Thomsen et al.* [2013] surveyed the dusk orbits of Cassini in 2010 and, other than strong downtail flows relatively near the magnetopause, found no evidence for outward flow in this region. They interpreted this to mean that Vasyliunas-style reconnection may have occurred on the dusk flank but that these plasmoids are still trapped within outer closed field lines and thus not free to escape downtail until they reach the postmidnight sector. It may also be that Cassini did not sample far enough downtail in this portion of its orbit to observe reconnection outflow (note that their data set had no measurements beyond $X_{KSM} \sim -20 R_S$ in the premidnight sector). In section 3 above, we present new plasma data showing the composition and velocity of a plasmoid on day 60 of 2006 at a local time of 2.3 h. These measurements indicated that this plasmoid contained plasma from an inner magnetospheric source and was traveling with a total velocity of ~ 170 km/s, of which ~ 90 km/s was in the radial direction.

5.4. What is the Morphology of the Reconnection Region?

In section 4, we explored the morphology of the reconnection regions, applying MVA to three tailward moving plasmoids to ascertain the direction of motion and to search for evidence of loop-like or flux rope-like structures. We saw a mix of examples: one with a loop-like geometry, one with a flux rope-like geometry, and one where the trajectory of the spacecraft through the outer portions of the plasmoid precludes a determination of a flux-rope-like or loop-like central structure. What yields these particular geometries in the first place?

A possible reason quoted in the literature for the production of flux rope-type plasmoids is simultaneous or sequential multiple x -line reconnection associated with substorms [e.g., *Elphic et al.*, 1986; *Slavin et al.*, 2003a; *Deng et al.*, 2004]. However, the single-spacecraft Cassini measurements do not allow us to observe multiple reconnection sites in the tail at once, and to date, no measurements of the x -line region itself have been made at Saturn. We note that the idea of a near-planet x line and a distant-tail x line is a popular picture in the terrestrial magnetosphere. However, this is one which again we are unable to directly infer from Cassini data. We suggest that the reconnection events shown in this paper are all associated with a near-Saturn reconnection site. All are within $68 R_S$ of the planet, which, by a simple scaling, is analogous to the region inside $30 R_E$ at Earth. The distant-tail x line at Earth is thought to be situated beyond $\sim 100 R_E$. Thus, we cannot know, based on our current data set, whether multiple x lines exist at different radial distances in Saturn’s tail, and hence, we cannot conclude anything regarding their potential influence on interior plasmoid structure.

The presence of a cross-tail magnetic field has been shown to be an important factor in the formation of flux rope-like plasmoids [Liu *et al.*, 2013], and suggestion made that this can come about via penetration of the azimuthal component of the interplanetary magnetic field (IMF) into the magnetosphere [e.g., Moldwin and Hughes, 1992]. Magnetic shear in the magnetotail can arise due to solar wind-magnetosphere coupling via magnetic reconnection at the dayside magnetopause. Due to the combination of frozen-in-flux and solar rotation, the IMF becomes increasingly tightly wound with increasing radial distance from the Sun. At 1 AU, this “Parker spiral angle” is $\sim 45^\circ$, but by the time the solar wind reaches ~ 9 AU, the field is strongly azimuthal, with an average angle of $\sim 83^\circ$ [Jackman *et al.*, 2008b]. However, the strength of the IMF at Saturn’s orbit is considerably weakened compared to that at Venus, Earth, and Mars. Perhaps the IMF at Saturn is not always sufficiently strong to impose a significant B_y component on the entire magnetosphere, especially given that it is competing against internal rotational dynamics for magnetospheric influence. In the case where Saturn’s magnetotail lobes are not sheared to the degree that they are at other planets, flux rope-like plasmoids would be much less likely to be formed.

A second aspect to consider is whether the plasmoids that Cassini observes are the result of reconnection involving open field lines. Early theoretical work at Earth explored the differences in magnetic topology introduced by reconnection on closed versus open field lines [e.g., Schindler, 1974; Hones, 1977]. Magnetic loops were achievable, at least in two dimensions, from reconnection of antiparallel field lines from opposite lobes at a single x line [e.g., Slavin *et al.*, 2003a]. Evidence for reconnection of open lobe field lines at Saturn was presented by Jackman *et al.* [2011]. However, we note that if the lobe magnetic field lines are significantly sheared relative to one another, this may make flux ropes more likely than loops.

Overall, our results on the interior morphology of plasmoids at Saturn are mixed. It is clear that during 2006, the hinging of the current sheet combined with the largely near-equatorial trajectory of the spacecraft has meant that Cassini typically passed through the bottom portion of plasmoids. This would, for example, reduce the duration of the encounters relative to the duration of a pass through the center of the structure and make it likely that the measurements failed to capture the actual core of the structures encountered. Thus, any conclusions we may draw regarding plasmoid-like or flux rope-like structures must be tempered with the knowledge that the field signatures are highly sensitive to the spacecraft trajectory through the structures. Future work will focus on fitting the field signatures using sophisticated flux rope fitting methods such as those employed by Slavin *et al.* [2003a] and Kivelson and Khurana [1995] to discern the impact parameter and explore the statistical trends in plasmoid axis orientation.

6. Summary

The aim of this study was to provide a comprehensive description of the local effects of magnetic reconnection in Saturn’s magnetotail (e.g., changing magnetic topology and energization of electrons) and the “global” effects (e.g., mass loss and flux closure). In order to achieve this aim, we have surveyed the Cassini magnetometer and plasma spectrometer data from the deep tail orbits of 2006 and found 69 tailward moving plasmoids, 17 TCRs, and 13 planetward moving events. Events can occur in isolation, as previously reported, but can also be found in chains, likely linked to single-reconnection episodes. The vast majority of events observed were tailward of the x line, and those planetward of the x line were observed over a wide range of radial distances, making it impossible to derive a statistical separatrix and indicating that the x line at Saturn is highly mobile. The average plasmoid observed at Saturn has a duration of ~ 17.71 min, followed by an extended interval of northward field, interpreted as analogous to the terrestrial postplasmoid plasma sheet, representing a period of flux closure. The average TCR at Saturn is evidenced by a broad compression of the field and a small deflection in the north-south component of the field. The average TCR compression ratio is 18%. Several important case studies have been shown, including an example of two plasmoids and two TCRs in quick succession, suggested to be linked to a single-reconnection episode. Plasma data for one of these plasmoids indicate that it has a composition commensurate with an inner magnetospheric source, and it is traveling with a total velocity of 170 km/s. Plasma data from 29 of the plasmoids have been used to estimate a range in their length from 0.44 – $23.9 R_S$, and we estimate that reconnection episodes in Saturn’s tail can close between 0.26 and 2.2 GWb of flux. The refinement of the assumptions that are involved in these calculations will be the subject of future work. The morphology of the reconnection region has been explored using MVA, with both loop-like and flux rope-like topologies present, but with results highly sensitive to the

trajectory of the spacecraft through the structures. We suggest that the observations presented here likely represent the largest events, and we are not ruling out steadier, smaller-scale mass release, perhaps on the dusk flank where observations thus far have been relatively scarce. The study of mass release at Saturn is key to our understanding of global magnetospheric dynamics, and we hope that future orbits of the Cassini spacecraft will afford us more chances to look in detail at the fascinating kronian magnetotail.

Acknowledgments

C.M.J.'s work at UCL was supported by a Leverhulme Trust Early Career Fellowship and a Royal Astronomical Society Fellowship, and her work at Southampton was supported by a Royal Astronomical Society Fellowship until December 2013. C.M.J., J.A.S., and M.F.V. discussed this work within the International Space Science Institute team number 195 on "Investigating the Dynamics of Planetary Magnetotails," led by C.M.J. M.F.T. was supported by the NASA Cassini program through JPL contract 1243218 with the Southwest Research Institute. The Cassini project is managed by the Jet Propulsion Laboratory for the NASA. J.P.E. is supported by an STFC Advanced Fellowship at ICL.

M. Balikhin thanks the reviewers for their assistance in evaluating this paper.

References

- Angelopoulos, V., et al. (1996), Multipoint analysis of a bursty bulk flow event on April 11, 1985, *J. Geophys. Res.*, *101*, 4967–4989, doi:10.1029/95JA02722.
- Arridge, C. S., N. André, N. Achilleos, K. K. Khurana, C. L. Bertucci, L. K. Gilbert, G. R. Lewis, A. J. Coates, and M. K. Dougherty (2008), Thermal electron periodicities at 20R_s in Saturn's magnetosphere, *Geophys. Res. Lett.*, *35*, L15107, doi:10.1029/2008GL034132.
- Arridge, C. S., et al. (2009), Plasma electrons in Saturn's magnetotail: Structure, distribution and energisation, *Planet. Space Sci.*, *57*(14–15), 2032–2047, doi:10.1016/j.pss.2009.09.007.
- Arridge, C. S., et al. (2011), Periodic motion of Saturn's nightside plasma sheet, *J. Geophys. Res.*, *116*, A11205, doi:10.1029/2011JA016827.
- Badman, S. V., and S. W. H. Cowley (2007), Significance of Dungey cycle flows in Jupiter's and Saturn's magnetospheres, and their identification on closed equatorial field lines, *Ann. Geophys.*, *25*, 941–951, doi:10.5194/angeo-25-941-2007.
- Badman, S. V., E. J. Bunce, J. T. Clarke, S. W. H. Cowley, J.-C. Gérard, D. Grodent, and S. E. Milan (2005), Open flux estimates in Saturn's magnetosphere during the January 2004 Cassini-HST campaign, and implications for reconnection rates, *J. Geophys. Res.*, *110*, A11216, doi:10.1029/2005JA011240.
- Badman, S. V., C. M. Jackman, J. D. Nichols, J. T. Clarke, and J.-C. Gérard (2013), Open flux in Saturn's magnetosphere, *Icarus*, *231*, 137–145, doi:10.1016/j.icarus.2013.12.004.
- Bagenal, F., and P. A. Delamere (2011), Flow of mass and energy in the magnetospheres of Jupiter and Saturn, *J. Geophys. Res.*, *116*, A05209, doi:10.1029/2010JA016294.
- Baker, D. N., R. C. Anderson, R. D. Zwickl, and J. A. Slavin (1987), Average plasma and magnetic field variations in the distant magnetotail associated with near-Earth substorm effects, *J. Geophys. Res.*, *92*, 71–81, doi:10.1029/JA092iA01p00071.
- Baker, D. N., T. I. Pulkkinen, V. Angelopoulos, W. Baumjohann, and R. L. McPherron (1996), Neutral line model of substorms: Past results and present view, *J. Geophys. Res.*, *101*(A6), 12,975–13,010, doi:10.1029/95JA03753.
- Birn, J. (1989), Three-dimensional equilibria for the extended magnetotail and the generation of field-aligned current sheets, *J. Geophys. Res.*, *94*, 252–260, doi:10.1029/JA094iA01p00252.
- Borg, A. L., M. G. G. T. Taylor, and J. P. Eastwood (2012), Observations of magnetic flux ropes during magnetic reconnection in the Earth's magnetotail, *Ann. Geophys.*, *30*, 761–773.
- Briggs, J. A., D. A. Brain, M. L. Cartwright, J. P. Eastwood, and J. S. Halekas (2011), A statistical study of flux ropes in the Martian magnetospheres, *Planet. Space Sci.*, *59*, 1498–1505.
- Bunce, E. J., S. W. H. Cowley, D. M. Wright, A. J. Coates, M. K. Dougherty, N. Krupp, W. S. Kurth, and A. M. Rymer (2005), In situ observations of a solar wind compression-induced hot plasma injection in Saturn's tail, *Geophys. Res. Lett.*, *32*, L20504, doi:10.1029/2005GL022888.
- Chen, Y., T. W. Hill, A. M. Rymer, and R. J. Wilson (2010), Rate of radial transport of plasma in Saturn's inner magnetosphere, *J. Geophys. Res.*, *115*, A10211, doi:10.1029/2010JA015412.
- Cowley, S. W. H., E. J. Bunce, and R. Prangé (2004), Saturn's polar ionospheric flows and their relation to the main auroral oval, *Ann. Geophys.*, *22*, 1379–1394.
- Deng, X. H., H. Matsumoto, H. Kojima, T. Mukai, R. Anderson, W. Baumjohann, and R. Nakamura (2004), Geotail encounter with reconnection diffusion region in the Earth's magnetotail: Evidence of multiple X lines collisionless reconnection?, *J. Geophys. Res.*, *109*, A05206, doi:10.1029/2003JA010031.
- Dougherty, M. K., et al. (2004), The Cassini magnetic field investigation, *Space Sci. Rev.*, *114*, 331–383, doi:10.1007/s11214-004-1432-2.
- Dungey, J. W. (1961), Interplanetary magnetic field and the auroral zones, *Phys. Rev. Lett.*, *6*, 47–48.
- Eastwood, J. P., and S. A. Kiehas (2014), Origin and evolution of plasmoids and flux ropes in the magnetotails of Earth and Mars, in *Magnetotails in the Solar System*, edited by A. Kieling, C. M. Jackman, and P. A. Delamere, AGU, Washington, D. C., in press.
- Eastwood, J. P., D. G. Sibeck, J. A. Slavin, M. L. Goldstein, B. Lavraud, M. Sitnov, S. Imber, A. Balogh, E. A. Lucek, and I. Dandouras (2005), Observations of multiple X-line structure in the Earth's magnetotail current sheet: A Cluster case study, *Geophys. Res. Lett.*, *32*, L11105, doi:10.1029/2005GL022509.
- Eastwood, J. P., et al. (2012), A chain of magnetic flux ropes in the magnetotail of Mars, *Geophys. Res. Lett.*, *39*, L03104, doi:10.1029/2011GL050444, ISSN:0094-8276.
- Elphic, R. C., and C. T. Russell (1983), Magnetic flux ropes in the Venus ionosphere: Observations and models, *J. Geophys. Res.*, *88*, 58–72, doi:10.1029/JA088iA01p00058.
- Elphic, R. C., and D. J. Southwood (1987), Simultaneous measurements of the magnetopause and flux transfer events at widely separated sites by AMPTE UKS and ISEE 1 and 2, *J. Geophys. Res.*, *92*, 13,666–13,672, doi:10.1029/JA092iA12p13666.
- Elphic, R. C., C. A. Cattell, K. Takahashi, S. J. Bame, and C. T. Russell (1986), ISEE-1 and 2 observations of magnetic flux ropes in the magnetotail: FTE's in the plasma sheet?, *Geophys. Res. Lett.*, *13*, 648–651, doi:10.1029/GL013i007p00648.
- Farrugia, C. J., R. C. Elphic, D. J. Southwood, and S. W. H. Cowley (1987), Field and flow perturbations outside the reconnected field region in flux transfer events: Theory, *Planet. Space Sci.*, *35*(2), 227–240.
- Fleshman, B. L., P. A. Delamere, and F. Bagenal (2010), The source of Saturn's extended neutral cloud, Abstract SM11C-1768 presented at 2010 Fall Meeting, AGU, San Francisco, Calif., 13–17 Dec.
- Henderson, P. D., C. J. Owen, I. V. Alexeev, J. Slavin, A. N. Fazakerley, E. Lucek, and H. Rème (2006), Cluster observations of flux rope structures in the near-tail, *Ann. Geophys.*, *24*, 651–666.
- Hesse, M., and M. G. Kivelson (1998), The formation and structure of flux ropes in the magnetotail, in *New Perspectives on the Earth's Magnetotail*, *Geophys. Monogr. Ser.*, vol. 105, edited by A. Nishida, D. N. Baker, and S. W. H. Cowley, pp. 139–151, AGU, Washington, D. C., doi:10.1029/GM105p0139.
- Hill, T. W., et al. (2008), Plasmoids in Saturn's magnetotail, *J. Geophys. Res.*, *113*, A01214, doi:10.1029/2007JA012626.
- Hones, E. W., Jr. (1976), The magnetotail: its generation and dissipation, in *Physics of Solar Planetary Environments*, vol. 2, edited by D. J. Williams, pp. 558–571, AGU, Washington, D. C.

- Hones, E. W., Jr. (1977), Substorm processes in the magnetotail: Comments on "On hot tenuous plasma, fireballs, and boundary layers in the Earth's magnetotail" by L.A. Frank et al., *J. Geophys. Res.*, **82**, 5633–5640, doi:10.1029/JA082i035p05633.
- Hsu, T.-S., and R. L. McPherron (2003), Occurrence frequencies of IMF triggered and nontriggered substorms, *J. Geophys. Res.*, **108**(A7), 1307, doi:10.1029/2002JA009442.
- Hughes, W. J., and D. G. Sibeck (1987), On the 3-dimensional structure of plasmoids, *Geophys. Res. Lett.*, **14**, 636–639, doi:10.1029/GL014i006p00636.
- Ieda, A., S. Machida, T. Mukai, Y. Saito, T. Yamamoto, A. Nishida, T. Terasawa, and S. Kokubun (1998), Statistical analysis of the plasmoid evolution with GEOTAIL observations, *J. Geophys. Res.*, **103**, 4435–4465, doi:10.1029/97JA03240.
- Imber, S. M., J. A. Slavin, H. U. Auster, and V. Angelopoulos (2011), A THEMIS survey of flux ropes and travelling compression regions: Location of the near-Earth reconnection site during solar minimum, *J. Geophys. Res.*, **116**, A02201, doi:10.1029/2010JA016026.
- Jackman, C. M., and C. S. Arridge (2011), Statistical properties of the magnetic field in the Kronian magnetotail lobes and current sheet, *J. Geophys. Res.*, **116**, A05224, doi:10.1029/2010JA015973.
- Jackman, C. M., C. T. Russell, D. J. Southwood, C. S. Arridge, N. Achilleos, and M. K. Dougherty (2007), Strong rapid dipolarizations in Saturn's magnetotail: In situ evidence of reconnection, *Geophys. Res. Lett.*, **34**, L11203, doi:10.1029/2007GL029764.
- Jackman, C. M., et al. (2008a), A multi-instrument view of tail reconnection at Saturn, *J. Geophys. Res.*, **113**, A11213, doi:10.1029/2008JA013592.
- Jackman, C. M., R. J. Forsyth, and M. K. Dougherty (2008b), The overall configuration of the interplanetary magnetic field upstream of Saturn as revealed by Cassini observations, *J. Geophys. Res.*, **113**, A08114, doi:10.1029/2008JA013083.
- Jackman, C. M., C. S. Arridge, H. J. McAndrews, M. G. Henderson, and R. J. Wilson (2009), Northward field excursions in Saturn's magnetotail and their relationship to magnetospheric periodicities, *Geophys. Res. Lett.*, **36**, L16101, doi:10.1029/2009GL039149.
- Jackman, C. M., J. A. Slavin, and S. W. H. Cowley (2011), Cassini observations of plasmoid structure and dynamics: Implications for the role of magnetic reconnection in magnetospheric circulation at Saturn, *J. Geophys. Res.*, **116**, A10212, doi:10.1029/2011JA016682.
- Jia, X., K. C. Hansen, T. I. Gombosi, M. G. Kivelson, G. Tóth, D. L. DeZeeuw, and A. J. Ridley (2012), Magnetospheric configuration and dynamics of Saturn's magnetosphere: A global MHD simulation, *J. Geophys. Res.*, **117**, A05225, doi:10.1029/2012JA017575.
- Jurac, S., and J. D. Richardson (2005), A self-consistent model of plasma and neutrals at Saturn: Neutral cloud morphology, *J. Geophys. Res.*, **110**, A09220, doi:10.1029/2004JA010635.
- Kanani, S. J., et al. (2010), A new form of Saturn's magnetopause using a dynamic pressure balance model, based on in situ, multi-instrument Cassini measurements, *J. Geophys. Res.*, **115**, A06207, doi:10.1029/2009JA014262.
- Kellett, S., E. J. Bunce, A. J. Coates, and S. W. H. Cowley (2009), Thickness of Saturn's ring current determined from north-south Cassini passes through the current layer, *J. Geophys. Res.*, **114**, A04209, doi:10.1029/2008JA013942.
- Kidder, A., C. S. Paty, R. M. Winglee, and E. M. Harnett (2012), External triggering of plasmoid development at Saturn, *J. Geophys. Res.*, **117**, A07206, doi:10.1029/2012JA017625.
- Kivelson, M. G., and K. K. Khurana (1995), Models of flux ropes embedded in a Harris neutral sheet: Force-free solutions in low and high beta plasmas, *J. Geophys. Res.*, **100**(A12), 23,657–23,645.
- Kivelson, M. G., and D. J. Southwood (2005), Dynamical consequences of two modes of centrifugal instability in Jupiter's outer magnetosphere, *J. Geophys. Res.*, **110**, A12209, doi:10.1029/2005JA011176.
- Kronberg, E. A., J. Woch, N. Krupp, and A. Lagg (2008), Mass release process in the Jovian magnetosphere: Statistics on particle burst parameters, *J. Geophys. Res.*, **113**, A10202, doi:10.1029/2008JA013332.
- Lepping, R. P., J. A. Jones, and L. F. Burgala (1990), Magnetic field structure of interplanetary magnetic clouds at 1 AU, *J. Geophys. Res.*, **95**, 11,957–11,965, doi:10.1029/JA095iA08p11957.
- Lepping, R. P., D. H. Fairfield, J. Jones, L. A. Frank, W. R. Paterson, S. Kokubun, and T. Yamamoto (1995), Cross-tail magnetic flux ropes as observed by the Geotail spacecraft, *Geophys. Res. Lett.*, **22**, 1193–1196, doi:10.1029/94GL01114.
- Li, S.-S., V. Angelopoulos, A. Runov, S. A. Kiehas, and X.-Z. Zhou (2013), Plasmoid growth and expulsion revealed by two-point ARTEMIS observations, *J. Geophys. Res. Space Physics*, **118**, 2133–2144, doi:10.1002/jgra.50105.
- Liu, C., X. Feng, J. Guo, and Y. Ye (2013), Study of small-scale plasmoid structures in the magnetotail using Cluster observations and Hall MHD simulations, *J. Geophys. Res. Space Physics*, **118**, 2087–2100, doi:10.1002/jgra.50248.
- Lundquist, S. (1950), Magnetohydrostatic field, *Ark. Fys.*, **2**, 361–365.
- Masters, A., M. F. Thomsen, S. V. Badman, C. S. Arridge, D. T. Young, A. J. Coates, and M. K. Dougherty (2011), Supercorotating return flow from reconnection in Saturn's magnetotail, *Geophys. Res. Lett.*, **38**, L03103, doi:10.1029/2010GL046149.
- McAndrews, H. J., et al. (2009), Plasma in Saturn's nightside magnetosphere and the implications for global circulation, *Planet. Space Sci.*, **57**(14–15), 1714–1722, doi:10.1016/j.pss.2009.03.003.
- Mitchell, D. G., et al. (2005), Energetic ion acceleration in Saturn's magnetotail: Substorms at Saturn?, *Geophys. Res. Lett.*, **32**, L20501, doi:10.1029/2005GL022647.
- Moldwin, M., and W. Hughes (1992), On the Formation and Evolution of Plasmoids: A Survey of ISEE 3 Geotail Data, *J. Geophys. Res.*, **97**, 19,259–19,282, doi:10.1029/92JA01598.
- Moldwin, M. B., J. L. Phillips, J. T. Gosling, E. E. Scime, D. J. McComas, S. J. Barne, A. Balogh, and R. J. Forsyth (1995), Ulysses observations of a noncoronal mass ejection flux rope: evidence of interplanetary magnetic reconnection, *J. Geophys. Res.*, **100**(19), 903–910.
- Paschmann, G., and P. Daly (Eds.) (1998), Analysis methods for multi-spacecraft data, ISSI Science Report, SR-001.
- Pontius, D., and T. W. Hill (2009), Inertial corotation lag and mass loading in Saturn's magnetosphere, *Geophys. Res. Lett.*, **36**, L23103, doi:10.1029/2009GL041030.
- Provan, G., D. J. Andrews, C. S. Arridge, A. J. Coates, S. W. H. Cowley, G. Cox, M. K. Dougherty, and C. M. Jackman (2012), Dual periodicities in planetary-period magnetic field oscillations in Saturn's tail, *J. Geophys. Res.*, **117**, A01209, doi:10.1029/2011JA017104.
- Richardson, I. G., S. W. H. Cowley, E. W. Hones Jr., and S. J. Bame (1987), Plasmoid-associated energetic ion bursts in the deep geomagnetic tail: Properties of plasmoids and the post-plasmoid plasma sheet, *J. Geophys. Res.*, **92**, 9997–10,013, doi:10.1029/JA092iA09p09997.
- Runov, A., et al. (2006), Local structure of the magnetotail current sheet: 2001 Cluster observations, *Ann. Geophys.*, **24**, 247–262.
- Russell, C. T. (1990), Magnetic Flux Ropes in the Ionosphere of Venus, in *Physics of Magnetic Flux Ropes*, *Geophys. Monogr. Ser.*, vol. 58, edited by C. T. Russell, E. R. Priest, and L. C. Lee, pp. 413–213, AGU, Washington, D. C.
- Russell, C. T., and R. C. Elphic (1979), Observations of magnetic flux ropes in the Venus ionosphere, *Nature*, **279**, 616–618.
- Russell, C. T., C. M. Jackman, H. Y. Wei, C. Bertucci, and M. K. Dougherty (2008), Titan's influence on Saturnian substorm occurrence, *Geophys. Res. Lett.*, **35**, L12105, doi:10.1029/2008GL034080.
- Schindler, K. (1974), A theory of the substorm mechanism, *J. Geophys. Res.*, **79**, 2803–2810, doi:10.1029/JA079i019p02803.
- Sergis, N., C. S. Arridge, S. M. Krimigis, D. G. Mitchell, A. M. Rymer, D. C. Hamilton, N. Krupp, M. K. Dougherty, and A. J. Coates (2011), Dynamics and seasonal variations in Saturn's magnetospheric plasma sheet, as measured by Cassini, *J. Geophys. Res.*, **116**, A04203, doi:10.1029/2010JA016180.

- Sibeck, D. G., G. L. Siscoe, J. A. Slavin, E. J. Smith, S. J. Bame, and F. L. Scarf (1984), Magnetotail flux ropes, *Geophys. Res. Lett.*, *11*, 1090–1093, doi:10.1029/GL011i010p01090.
- Slavin, J., E. Smith, B. Tsurutani, D. Sibeck, H. Singer, D. Baker, J. Gosling, E. Hones, and F. Scarf (1984), Substorm-associated traveling compression regions in the distant tail: ISEE-3 geotail observations, *Geophys. Res. Lett.*, *11*, 657–660, doi:10.1029/GL011i007p00657.
- Slavin, J. A., E. J. Smith, D. G. Sibeck, D. N. Baker, R. D. Zwickl, and S.-I. Akasofu (1985), An ISEE 3 study of average and substorm conditions in the distant magnetotail, *J. Geophys. Res.*, *90*, 10,875–10,895, doi:10.1029/JA090iA11p10875.
- Slavin, J. A., et al. (1989), CDAW-8 observations of plasmoid signatures in the geomagnetic tail: An assessment, *J. Geophys. Res.*, *94*, 15,153–15,175, doi:10.1029/JA094iA11p15153.
- Slavin, J. A., M. F. Smith, E. L. Mazur, D. N. Baker, E. W. Hones Jr., T. Iyemori, and E. W. Greenstadt (1993), ISEE 3 Observations of Travelling Compression Regions in the Earth's Magnetotail, *J. Geophys. Res.*, *98*(A9), 15,425–15,446, doi:10.1029/93JA01467.
- Slavin, J. A., C. J. Owen, M. M. Kuznetsova, and M. Hesse (1995), ISEE 3 observations of plasmoids with flux rope magnetic topologies, *Geophys. Res. Lett.*, *22*(15), 2061–2064, doi:10.1029/95GL01977.
- Slavin, J. A., R. P. Lepping, J. Gjerloev, D. H. Fairfield, M. Hesse, C. J. Owen, M. B. Moldwin, T. Nagai, A. Ieda, and T. Mukai (2003a), Geotail observations of magnetic flux ropes in the plasma sheet, *J. Geophys. Res.*, *108*(A1), 1015, doi:10.1029/2002JA009557.
- Slavin, J. A., et al. (2003b), Cluster four spacecraft measurements of small traveling compression regions in the near-tail, *Geophys. Res. Lett.*, *30*(23), 2208, doi:10.1029/2003GL018438.
- Slavin, J. A., E. I. Transkanen, M. Hesse, C. J. Owen, M. W. Dunlop, S. Imber, E. A. Lucek, A. Balogh, and K.-H. Glassmier (2005), Cluster observations of traveling compression regions in the near-tail, *J. Geophys. Res.*, *110*, A06207, doi:10.1029/2004JA010878.
- Sonnerup, B. U. O., and L. J. Cahill jr. (1967), Magnetopause structure and attitude from Explorer 12 observations, *J. Geophys. Res.*, *72*, 171–183, doi:10.1029/JZ072i001p00171.
- Szego, K., Z. Nemeth, G. Erdos, L. Foldy, Z. Bebesi, M. Thomsen, and D. Delapp (2012), Location of the magnetodisk in the nightside outer magnetosphere of Saturn near equinox based on ion densities, *J. Geophys. Res.*, *117*, A09225, doi:10.1029/2012JA017817.
- Thomsen, M. F., R. J. Wilson, R. L. Tokar, D. B. Reisenfeld, and C. M. Jackman (2013), Cassini/CAPS observations of duskside tail dynamics at Saturn, *J. Geophys. Res. Space Physics*, *118*, 5767–5781, doi:10.1002/jgra.50552.
- Thomsen, M. F., C. M. Jackman, R. L. Tokar, and R. J. Wilson (2014), Plasma Flows in Saturn's Nightside Magnetosphere, *J. Geophys. Res. Space Physics*, *119*, doi:10.1002/2014JA019912.
- Vasyliunas, V. M. (1983), Plasma distribution and flow, in *Physics of the Jovian Magnetosphere*, edited by A. J. Dessler, pp. 395–453, Cambridge Univ. Press, New York, doi:10.1017/CBO9780511564574.013.
- Vogt, M. F., M. G. Kivelson, K. K. Khurana, S. P. Joy, and R. J. Walker (2010), Reconnection and flows in the Jovian magnetotail as inferred from magnetometer observations, *J. Geophys. Res.*, *115*, A06219, doi:10.1029/2009JA015098.
- Vogt, M. F., C. M. Jackman, J. A. Slavin, E. J. Bunce, S. W. H. Cowley, M. G. Kivelson, and K. K. Khurana (2014), Structure and Statistical Properties of Plasmoids in Jupiter's Magnetotail, *J. Geophys. Res. Space Physics*, *119*, 821–843, doi:10.1002/2013JA019393.
- Volwerk, M., et al. (2013), Comparative magnetotail flapping: an overview of selected events at Earth, Jupiter and Saturn, *Ann. Geophys.*, *31*, 817–833, doi:10.5194/angeo-31-817-2013.
- Woch, J., N. Krupp, and A. Lagg (2002), Particle bursts in the Jovian magnetosphere: Evidence for a near-Jupiter neutral line, *Geophys. Res. Lett.*, *29*(7), 1138, doi:10.1029/2001GL014080.
- Zhang, H., et al. (2010), Evidence that crater flux transfer events are initial stages of typical flux transfer events, *J. Geophys. Res.*, *115*, A08229, doi:10.1029/2009JA015013.
- Zhang, H., M. G. Kivelson, V. Angelopoulos, K. K. Khurana, Z. Y. Pu, R. J. Walker, R. L. McPherron, T.-S. Hsu, Q. G. Zong, and T. Phan (2012), Generation and properties of in vivo flux transfer events, *J. Geophys. Res.*, *117*, A05224, doi:10.1029/2011JA017166.
- Zieger, B., K. C. Hansen, T. I. Gombosi, and D. L. De Zeeuw (2010), Periodic plasma escape from the mass-loaded Kronian magnetosphere, *J. Geophys. Res.*, *115*, A08208, doi:10.1029/2009JA014951.
- Zong, Q.-G., et al. (2004), Cluster observations of earthward flowing plasmoid in the tail, *Geophys. Res. Lett.*, *31*, L18803, doi:10.1029/2004GL020692.